JAERI-M
8624

IAEA INTOR WORKSHOP REPORT, GROUP 11
—— STABILITY CONTROL ——

January 1980

Fusion Research and Development Center

日本原子力研究所
Japan Atomic Energy Research Institute

この報告書は，日本原子力研究所が JAERI-M レポートとして，不定期に刊行している研究報告書です．入手，複製などのお問合わせは，日本原子力研究所技術情報部（茨城県那珂郡東海村）あて，お申しこしください．

JAERI-M reports, issued irregularly, describe the results of research works carried out in JAERI. Inquiries about the availability of reports and their reproduction should be addressed to Division of Technical Information, Japan Atomic Energy Research Institute, Tokai-mura, Naka-gun, Ibaraki-ken, Japan.

JAERI-M 8624

IAEA INTOR Workshop Report, Group 11
- Stability Control -

Fusion Research and Development Center,
Tokai Research Establishment, JAERI
(Received December 19, 1979)

Data base assessments of INTOR are presented. Included are the theoretical β-limits, experimental results of current disruption in DIVA, wide range of parameter study of plasma shaping, effect of conducting shell on positional and ballooning mode, and the method of disruption control. Good shell effect of the SS blanket is examined. Also shown is the possibility of the equilibrium control of minor radius expansion. Design of hybrid poloidal coil system with exterior coils has been carried out.

Keyword: INTOR Tokamak Reactors, Stability Control, Current Disruption, Hybrid Poloidal Coils, Plasma Shaping, Data Base Assessment

---

Prepared by: Tatsuoki TAKEDA (Group leader), Genichi KURITA, Toshihiko MATSUURA*1, Hiromasa NINOMIYA, Toshihide TSUNEMATSU, Ryuichi SHIMADA, Kichiro SHINYA*2

*1 On leave from Fujitsu Ltd.

*2 On leave from Toshiba Corp.

JAERI-M 8624

IAEA INTORワークショップ検討報告書・グループ11
―― 安定性制御 ――

日本原子力研究所東海研究所
核融合研究開発推進センター

（1979年12月19日受理）

INTORのプラズマ安定性制御についてのデータベースの評価を行った。その内容は，理論的なベータ値の上限の推定，DIVAにおけるディスラプションの実験結果，広いパラメータに渡るプラズマ成形の検討，位置不安定およびバルーニング・モードに対する導体壁の安定化効果，ディスラプションの抑制法等である。INTORに使用されるSUSブランケットが，良好な導体壁効果を有し，プラズマの安定性に寄与することが示された。平衡とプラズマ形状を維持しながら，プラズマ小半径を拡大することが可能であることが検証された。以上の検討を基礎にしてトロイダルコイルの外側にのみコイルを配置するハイブリッド・コイルの設計を行った。

執筆者：竹田　辰興（グループリーダ）・栗田　源一・松浦　俊彦[*1]
二宮　博正・常松　俊秀・嶋田　隆一・新谷　吉郎[*2]

＊1　外来研究員　富士通㈱
＊2　外来研究員　東京芝浦電気㈱

CONTENTS

(edited by K. Shinya)

目　　次

（新谷吉郎編）

1. Introduction and Summary

1.1 How much multipole field components is required for INTOR equilibrium?

Systematic studies on the plasma equilibrium without divertor have been carried out for various poloidal betas, triangularities and current profiles of the plasma. The dependence of the quadrupole and the hexapole magnetic field on the poloidal beta and triangularity is formulated as follows,

$$B_q = g_1(\gamma) - g_2\beta_p$$

$$B_h = k_1\gamma - k_2\beta_p + k_3 \ .$$

Octapole field is not necessary for a D-shaped plasma without divertor, but seems to be needed in the case of divertor configuration.

1.2 Can theoretical β-limit guarantee the INTOR?

The theoretical β-limit of the INTOR has been analysed from the stability criteria for linear ideal MHD instabilities by using the ERATO and BOREAS code.

The external n = 1 mode instability is completely stabilized and the n = 2 mode determines the beta-limit if the position of the conducting wall is less than about 1.2 times of the plasma radius. In the case of equilibria with TT'∝p' which are usually adopted for numerical analyses, the total beta value increases with increasing $\bar{\beta}_p$ in the range of lower $\bar{\beta}_p$, but sharply decreases in the parameter range of the INTOR. It is possible that some other sophisticated equilibria may give higher beta value for higher poloidal beta value. What kinds of equilibria among them are realizable depends on transport processes and this problem will be solved by using 1-1/2D(2D) tokamak codes. Triangularity of the plasma cross section improves the stability property and raises beta value considerably.

Total beta value $\bar{\beta}_t$ > 5-6% is expected to be attainable for the parameters of the INTOR.

1.3 What is the origin of the major disruption?

Concerning the origin of the major disruption the following results are obtained in DIVA experiments. (i) After reducing impurities, no major disruption is obtained. (ii) The disruptive instability does not

appear in $q_a < 2$ plasma which is stably obtained by reducing a radiation loss. (iii) Separatix stabilizes the surface mode and does not affect the major disruption.

It is concluded that the major disruption is induced by the impurity increase and the internal disruptions which enhance the m=2/n=1 mode.

The heat flux due to the major discuption can be easily controlled in a divertor device by broadening the thickness of the scrape-off layer.

1.4 Thick SS blanket will suppress the positional instability.

Elongation deteriorates the stability property of a plasma against the n = 0 axisymmetric mode. Without a conducting wall there is no positionally stable plasma equilibrium for any value of elongation. For $\Lambda \gtrsim 1.6$ (Λ is the ratio of wall radius to plasma radius) the critical value of elongation for the positional stability is about 1.5 but it depends slightly on the current profile and other plasma parameters.

The critical value of elongation for the positional stability becomes larger for smaller value of Λ and the plasma becomes unconditionally stable if the conducting wall is located sufficiently close as $\Lambda \lesssim 1.5$.

Positive value of δ(triangularity) improves the positional stability in the vicinity of the critical value of elongation but any triangular deformation deteriorates the positional stability for a plasma with small elongation.

The thick SS blanket equipped in INTOR can stabilize the positional instability and no feedback stabilization is necessary. But even in this case stability properties of a plasma which has separatrices in vacuum field close to the plasma surface should be examined.

If a blanket aiming at substantial tritium breeding is installed effective distance between the plasma and wall become large and Λ becomes $1.6 \sim 2.0$. In this case it is necessary to adopt an active feedback system or lower the ellipticity of the plasma.

1.5 Disruption can be suppressed by realizing a stable dischage with $q_a < 2$.

Considering magnitude of loss fluxes, major disruptions should be suppressed completely in the INTOR plasma.

Two different ways are possible to suppress the major disruptions.

(i) As the cause of the major disuption is considered to be the m=2/n=1 fluctuations the major disruption will be suppressed by realizing a stable discharge with $q_a < 2$. This will be possible by using the thick SS blanket.

(ii) For the same reason the major disruption will be suppressed by operating the device to sustain, always, the plasma profile which is stable against the m=2/n=1 fluctuations. This method is, in principle, possible but in this case some feedback controls of the plasma profile such as local heating of the plasma are needed.

No realistic method on an active feedback system for the disruption has been devised. Feedback control to sustain the stable profile against m=2/n=1 fluctuations is only practical control method for suppression of the major disruption. Even this feedback method, however, has many difficult problems from the engineering points of view. Therefore, low q_a operation ($q_a<2$) which absolutely suppresses the m=2/n=1 fluctuations seems more realistic for this purpose.

1.6 Profile control is important in INTOR

Some profile control is required so that we are able to realize an appropriate stable MHD equilibrium in order to attain a higher beta state. Density profile control will be done by gas and pellet injection. Current profile during current build-up can be controlled by expanding the plasma minor radius, while local heating of the plasma is needed to control current profile during plasma burning.

1.7 Current rise with minor radius expansion will be attained successfully.

Minor radius expansion seems to be most promising method to increase the plasma current without skin current. Equilibrium configurations with divertor during minor radius expansion can easily be obtained, and the time evolution of the multipole components of the field is studied for fixed triangularity of $\gamma = 0.2$. At low plasma current large hexapole and octapole magnetic field must be supplied. To lower the electric power requirement free-expansion-like minor radius expansion seems to be favourable.

1.8 Additional heating with gradual increase of triangularity is a natural method.

During additional heating vertical field must increase, while hexapole field may decrease with increasing β_p if the triangularity of the plasma cross section is hold constant. To avoid unnecessary change of coil currents it is to be desired that the triangularity of the plasma is increased with increasing β_p. This way reduces electric power and control requirement.

1.9 Exterior hybrid poloidal coils are the best selection

Emphasis should be laied on the engineering aspect in INTOR because of requirement of remote maintenance, existance of super conducting magnets, larger electromagnetic forces acting on coils, large access gap required for NBI and test modules and so on.

Exterior hybrid poloidal coils fullfil these requirements with some additive electric power compared with the interior or inner/outer hybrid coils. Poloidal divertor configuration is also realized with only exterior coils which remarkably improve the maintainability of the divertor.

Total ampere-turns of the exterior coils is about 10 times the plasma current, and the electric power required for start up is about 400 MVA (non divertor) or 700 MVA (divertor).

Change of magnetic field in the super conducting toroidal field coils can be reduced to a tolerable level by carefully arranging poloidal field coils, optimizing ampere-turns and increasing plasma current slowly.

Assessments of the interior coils are summarized in Table 1.1

Table 1.1

Interior Coils For	Measures
break down	necessary break down voltage can be reduced down to 50V by preionization, clean wall surface and small error field less than 50G, exterior SC coil can produce such voltage.
shaping	shaping can be controlled by exterior coils.
positional control n=1 kink mode defense of disruption	shielding with 30cm thickness ss has shell effect with 500-700ms time constant which stabilize positional and n=1 kink mode instabilities, and by which induced magnetic field in the toroidal coils at disruption is reduced by about 1/100.
m=1/n=1 tearing mode	major disruption might be suppressed by low q_a (<2) operation or by stabilizing m=2/n=1 mode with plasma distribution control.

2. Equilibrium and Plasma Shape

2.1 Method of calculation

The D-shaped plasma with appropriate triangularity has improved stability for positional and ballooning mode than the elliptic plasma as is shown in the Stability Control. Moreover, D-shape is a natural configuration for a high beta tokamak. Triangular form of the plasma is due to hexapole magnetic field, but the quantitative dependence of triangularity on the hexapole field has not been investigated yet. Systematic study on the relationships between the triangularity and the dipole, quadrupole and hexapole magnetic field in the wide range of poloidal beta values for the non-divertor configuration has been carried out. Studies on divertor configuration are put into practice now.

We choose a D-shaped plasma with a surface described by the following equations.

$$R = R_p + a\cos(\theta + \gamma \sin\theta)$$
$$Z = \kappa a \sin\theta \qquad (2\text{-}1)$$

where R_p and a are major and minor radii of the plasma respectively, and θ is a poloidal angle measured with respect to mid-plane.
Triangularity Δ is written in $\Delta = \sin\gamma$, and is approximated to γ, when γ is smaller than unity. Therefore γ is used as a triangularity in the following description without mention.

Poloidal magnetic field on the mid-plane can be resolved into multipole field components as is shown in eq. (2-2),

$$B_p(R) = B_v + B_q\frac{x}{R_p} + B_h\left(\frac{x}{R_p}\right)^2 + B_o\left(\frac{x}{R_p}\right)^3 + \cdots\cdots, \qquad (2\text{-}2)$$

dipole quad'pole hexapole octapole

where $x = R - R_p$. The decay index at the major radius of the plasma is written in $n = -B_q/B_v$ using above notation.

Multipole field has been analysed by using a free boundary equilibrium code which enable to adjust a flux surface to a required shape.[1)] Equilibrium is calculated for such a class as

$$\frac{dp}{d\Psi} = \lambda(\Psi-\Psi_s)^\alpha, \qquad \frac{\mu_o}{2}\frac{dI^2}{d\Psi} = \eta(\Psi-\Psi_s)$$
$$\frac{\eta}{\lambda} \simeq R_p^2\left(\frac{1}{\beta_J} - 1\right) \qquad (2\text{-}3)$$

where $p(\psi)$ is a plasma pressure and $I(\psi)$ is a poloidal current function. β_J is an approximate value of the poloidal beta. Exact poloidal beta is defined in the following form,

$$\beta_p = \frac{\int p ds / \int ds}{(\int B_p dl / \int dl)^2 / \mu_0} \tag{2-4}$$

In the equilibrium calculation code, β_p is converged to a required value by iteration.

The value of α, which is a measure of the plasma current peaking, is hold to 0.78 throughout the calculations. In this case the internal plasma inductance ℓ_i is nearly equal to unity which corresponds to almost quadratic plasma current distribution.

2.2 Dependence of multipole field on the poloidal beta and the triangularity

Fig. 2.1 shows the dependence of each multipole field on the triangularity for various poloidal beta values which correspond additional heating phase. Hexapole magnetic field, B_h, is directly proportional to the triangularity, and runs parallel with each other when the poloidal beta value is changed. Octapole field dose not exist in this model.

Equilibrium configurations obtained are shown in Fig. 2.2 indicating that the flux surface fits a required shape exactly.

Fig. 2.3 shows the critical triangularity, γ_0, and the base quadrupole field, B_{q0}, vs poloidal beta, where γ_0 is defined as the value at which hexapole field becomes zero, and B_{q0} is defined as the value for a elliptic cross section (γ=0). It can be concluded that for a D-shaped plasma, the shape of which surface is represented in eq. (2-1), the quadrupole and the hexapole field are written in the following quite simple forms,

$$\begin{aligned} B_q &= g_1(\gamma) - g_2 \beta_p \\ B_h &= k_1\gamma - k_2\beta_p + k_3 \ . \end{aligned} \tag{2-5}$$

The proportion coefficients g_2, k_1, k_2 and k_3 are supposed to be weak functions of the aspect ratio and/or ellipticity, and are equal to 0.03, 3.78, 0.18 and 0.06 respectively for the INTOR parameters. g_1 is also weakly dependent on the triangularity, but cannot be formulated exactly.

Fig. 2.4 shows B_V - n diagrams obtained from a number of parameter

studies for almost quadratic (α = 0.78, $\ell_i \simeq 1.0$) and more peaked plasma current distribution (α = 1.8, $\ell_i \simeq 1.6$).

The dependence of the safety factor at the plasma surface, q_a, on triangularity is shown in Fig. 2.5 with the poloidal beta as parameters. Safety factor on magnetic axis, q_0, is not always greater than unity, so stability problems should be verified in another way.

Any D-shaped plasma can be obtained if the multipole fields shown in Fig. 2.1 are realized by the practical poloidal field coil configuration.

2.3 Effect of plasma current peaking

It is very likely that the profile control of the plasma current might suppress the unstable m=2/n=1 mode. The dependence of the multipole fields on the current profile was investigated. The result is shown in Fig. 2.6. Dipole field B_v hardly changes because the radial position of the plasma can be decided by the total plasma current and the dipole field. Current peaking demands more quadrupole and hexapole magnetic field. This is because that the current near the surface is effective on the plasma shaping. Flat current profile requires less quadrupole and hexapole field resulting in the less electric power requirement for the poloidal field coils. Low q operation, which inevitably requires flat current profile, is favourable in this reason.

Reference

(1) H. Ninomiya, K. Shinya and A. Kameari; Optimization of Currents in Field-Shaping Coils of a Non-Circular Tokamak, 8th Symposium on Engineering Problems of Fusion Research (1979)

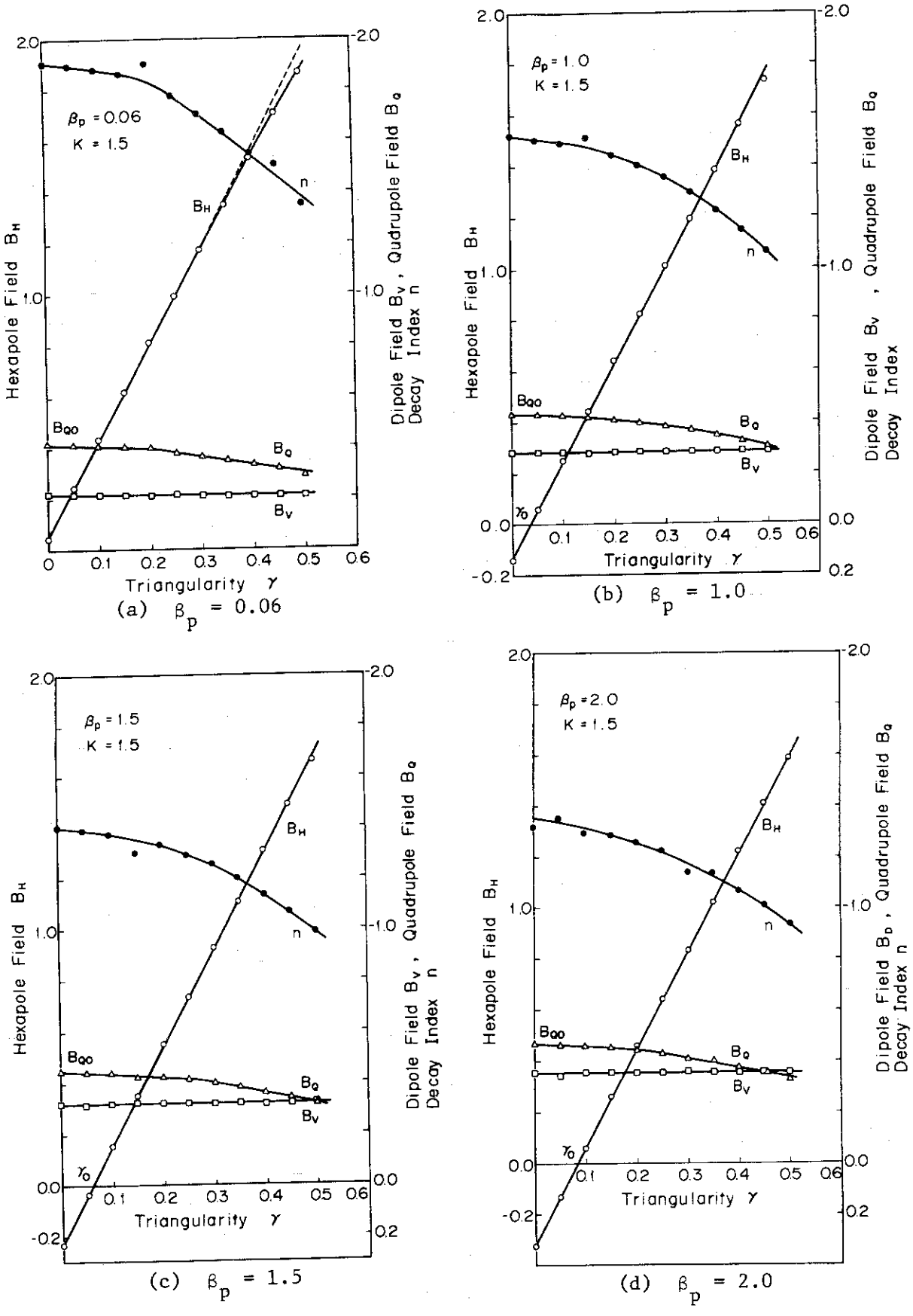

Fig. 2.1 Dependence of the multipole fields on the triangularity for various poloidal beta values. Equilibrium is calculated for the plasma having R_p=5.0 m, a=1.2 m and ellipticity K=1.5.

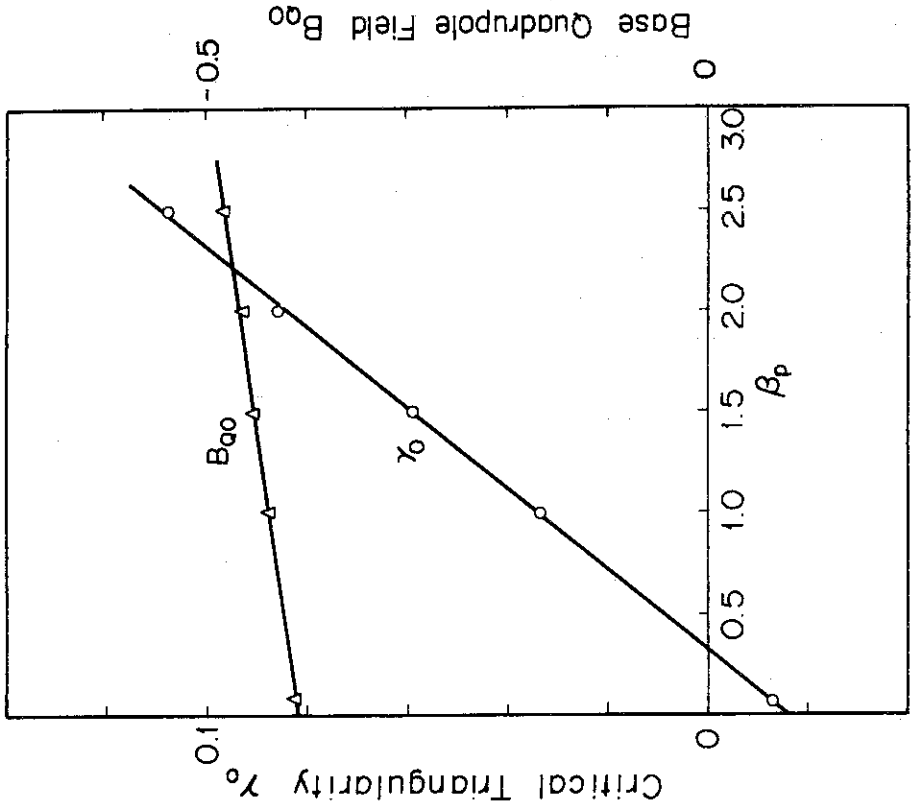

Fig. 2.3 Dependence of critical triangularity γ_0 and base quadrupole field B_{QO} on the poloidal beta value.

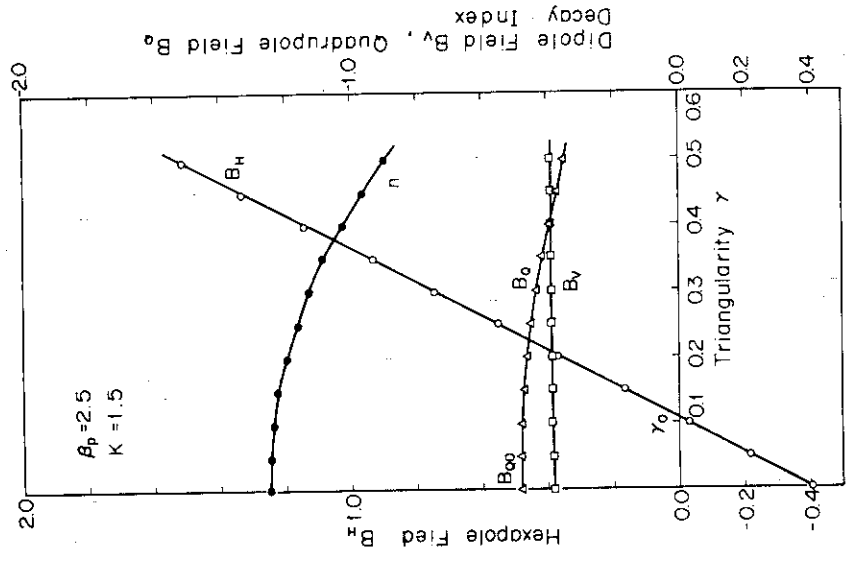

(e) β_p = 2.5

Fig. 2.1 continued

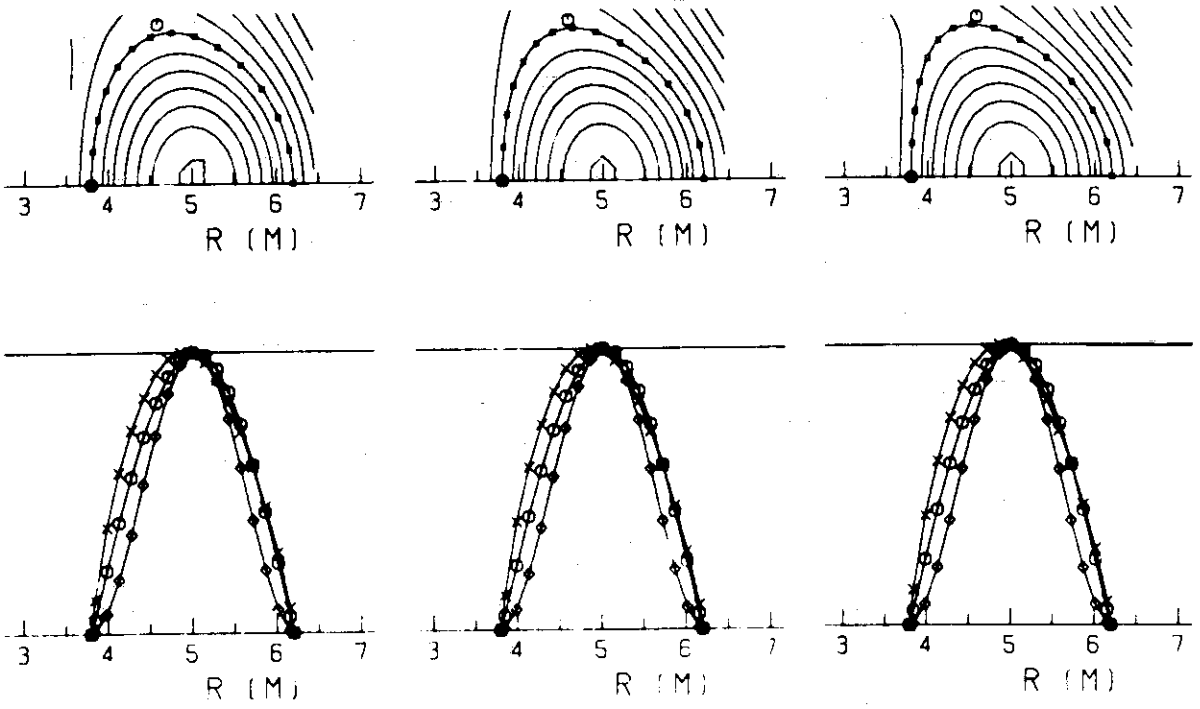

(a) β_p=0.06, γ=0.2 (b) β_p=0.06, γ=0.3 (c) β_p=0.06, γ=0.4

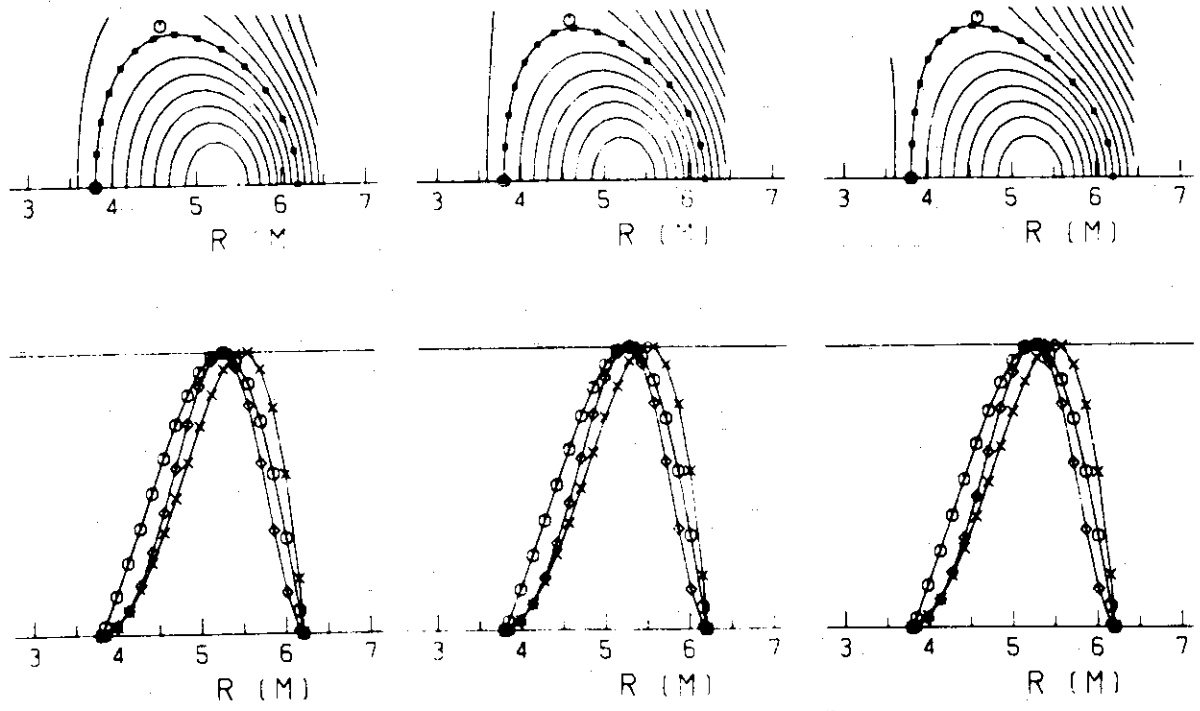

(d) β_p=2.5, γ=0.2 (e) β_p=2.5, γ=0.3 (f) β_p=2.5, γ=0.4

Fig. 2.2 Calculated equilibrium shape showing close fit to the required one. Also shown are the plasma current (—×—), pressure (—•—) and magnetic flux (—⊕—).

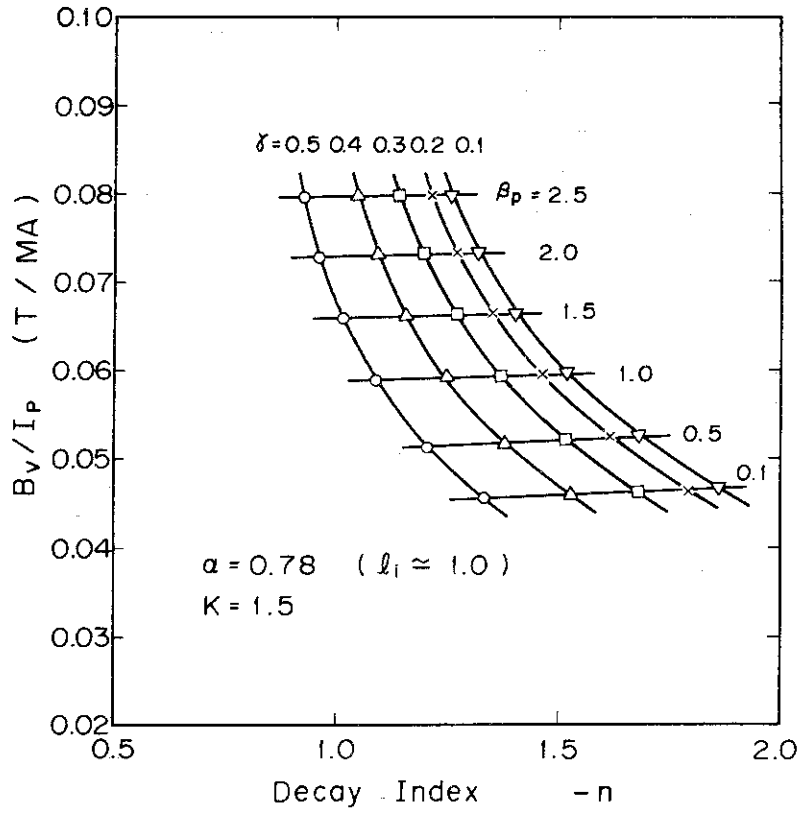

Fig. 2.4(a) B_V-n diagram for almost quadratic plasma current distribution. β_p is the poloidal beta, and γ is the triangularity of the plasma cross section.

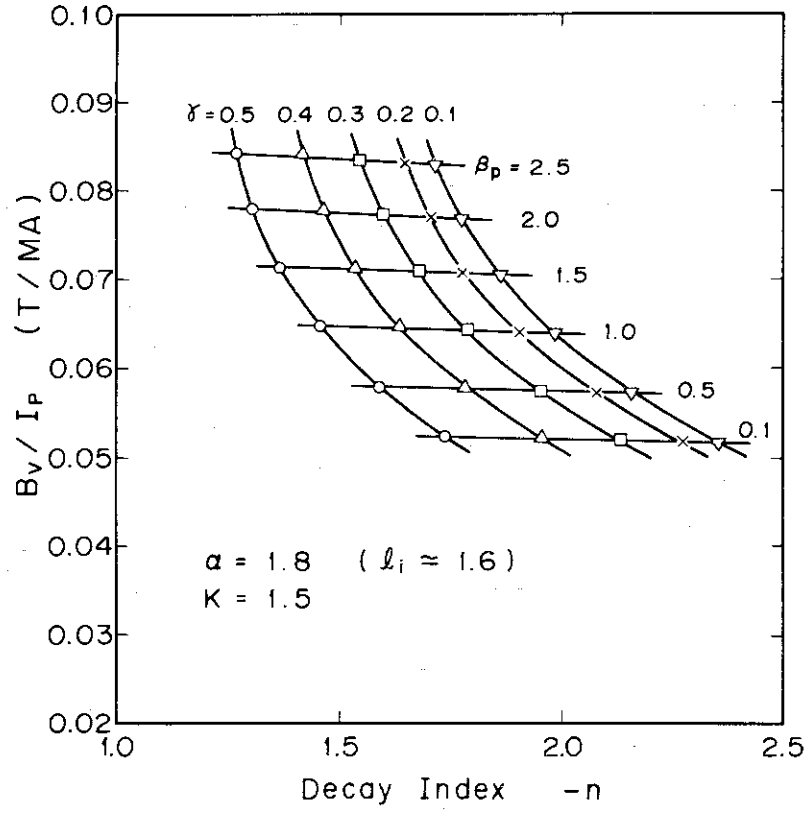

Fig. 2.4(b) B_V-n diagram for peaked plasma current distribution

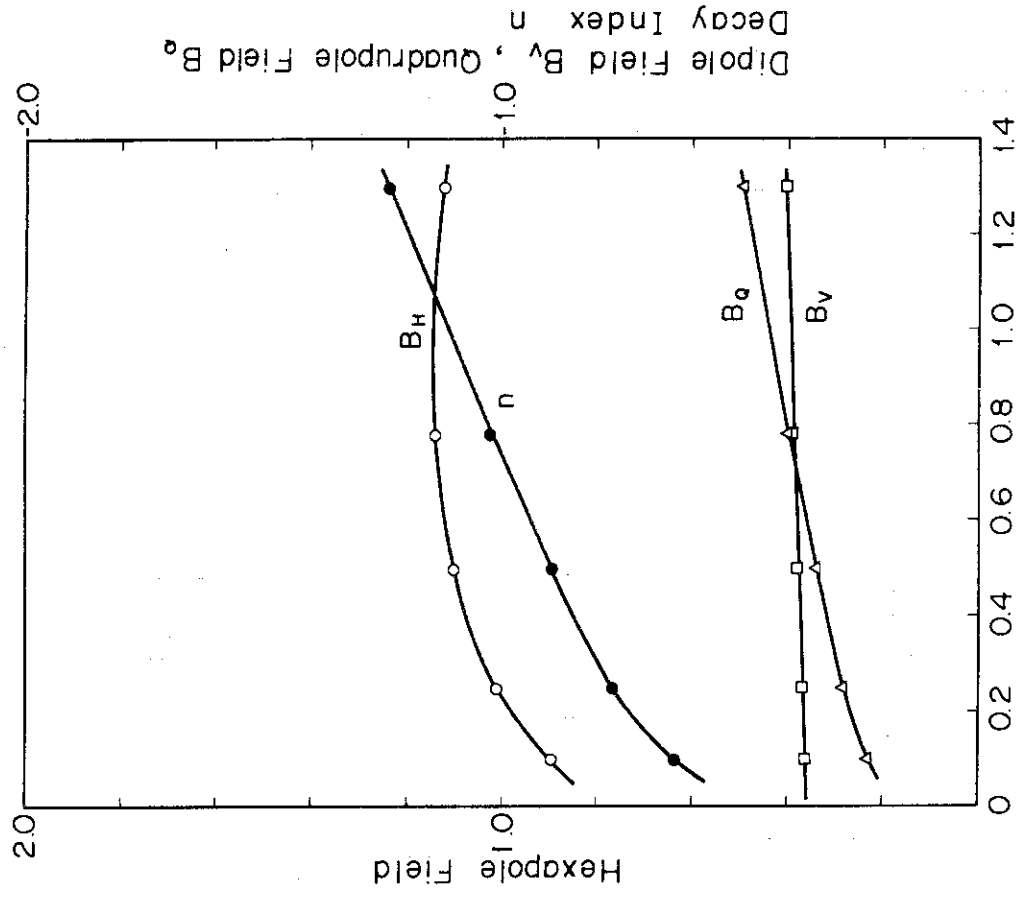

Fig. 2.6 Dependence of the multipole field on the plasma current profile.

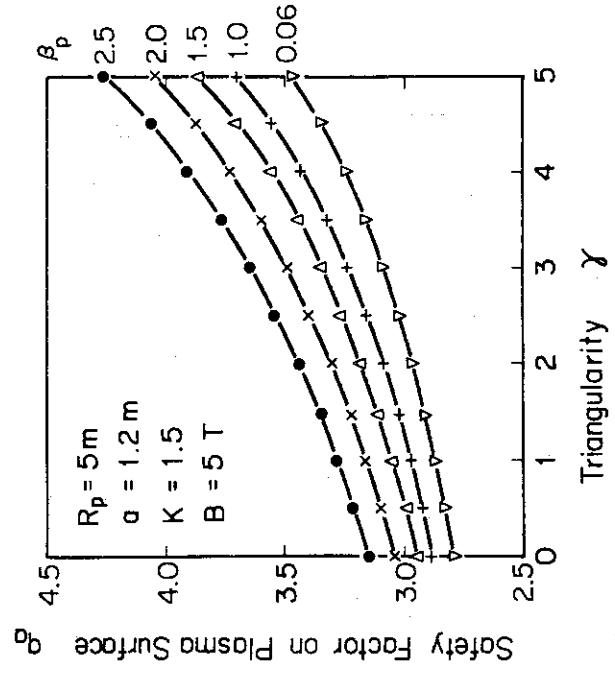

Fig. 2.5 Dependence of safety factor at the plasma surface on the triangularity with poloidal beta values as parameters.

3. Stability Limits on β

3.1 Theoretical β-limit

In this section we assess the theoretical β-limit of the INTOR from the stability criteria for linear ideal MHD instabilities. From the viewpoint of characteristics of unstable modes and, consequently, methods of solution, it is convenient to classify the instabilities into the following three categories:

i) Low mode number, internal and external instabilities

ii) High mode number, ballooning instabilities

iii) High mode number, localized (Mercier) instabilities

In a tokamak plasma, the Mercier criterion for stability of localized modes is well expressed as

$$q_o > q_{oc} \tag{3.1}$$

where q_o is the safety factor at the magnetic axis. The critical q_o value (q_{oc}) increases with increasing ellipticity of the plasma cross-section. In the case of a tokamak with a circular cross-section the critical value is about unity but in the case of the equilibrium class of our INTOR (E=1.5) calculation the critical value increases to about 1.2 which, naturally, depends slightly on a current profile and poloidal beta value. The critical value of q_o can be lowered by introducing a triangularity component to the shape of magnetic surfaces, and if we consider only this kind of instabilities very high β state will be possible.

The first and second classes of instabilities are more directly concerned with determination of the critical beta value.

3.1.1 Low-n mode instabilities

The low-n mode instabilities are analyzed by using the ERATO code[1]. A class of MHD equilibria investigated in this article is expressed by the following pressure (p) and toroidal field (T/r) profiles[2]:

$$P = \beta_J P_o' \{\psi - \frac{\alpha}{2}[(\psi-\psi_o)^2-\psi_o^2] + \frac{\gamma}{L+1}[(\psi-\psi_o)^{L+1}-(-\psi_o)^{L+1}]\} \tag{3-2}$$

$$\gamma = -\frac{1-\alpha\psi_o}{(-\psi_o)^L} \tag{3-3}$$

$$TT' = (\frac{1}{\beta_J}-1)P' \frac{1}{\langle \frac{1}{r^2} \rangle} \sim (\frac{1}{\beta_J}-1)R_o^2 P' \tag{3-4}$$

where ψ_o is the flux function at the magnetic axis, r is the major radius ($r=R_o$: position of the magnetic axis), and β_J is the approximate value of the poloidal beta. In our analyses, the minimum safety factor at the plasma boundary q_{bm} is searched for fixed $\bar{\beta}_p$ and q_o values, and then the maximum beta value is determined from the most stringent value among the results for the different β_J and toroidal mode number n. Parameter survey on the effects of aspect ratio (A), ellipticity (E) and triangularity (δ) is not carried out. Table 3-1. summarizes the values of the parameters for the analyses.

1) Effect of conducting wall

A conducting wall surrounding the plasma is effective to stabilize an external mode. This was numerically confirmed by Berger et al. for the case of a tokamak with the Solovév equilibrium[3] and by Tsunematsu et al. for the case of a conventional circular cross-section tokamak with a more realistic current profile[4]. According to the latter calculation the external n=1 mode instability is completely stabilized and the n=2 mode determines the beta-limit if the position of the conducting wall ($\Lambda=b/a$; b: radius of the wall, a: plasma minor radius) is less than about 1.2 (Fig. 3-1). In our analyses, we assume that a perfectly conducting wall is located at $\Lambda = 1.1$. Therefore, it will be safe to say that the n = 1 mode instability is strongly stabilized. It is also confirmed by the present analyses which shows that the beta value is determined by the n = 2 mode instabilities rather than the n = 1 ones (Fig. 3-2).

2) Dependence on the poloidal beta value

Generally the critical safety factor (q_{bc}) is increased by increasing the poloidal beta value. The total beta value, however, increases with the increase of $\bar{\beta}_p$ in the range of lower $\bar{\beta}_p$[5]. But it is found that the beta sharply decreases in the parameter range of the INTOR (Fig. 3-2). In the higher $\bar{\beta}_p$ case of the INTOR the instability of ballooning feature seems to determine the stability limit.

3) The critical beta value

As previously described the critical beta value is determined by the n = 2 mode instability rather than the n = 1 mode one. In Table 3-2 the critical points are summarized for β_J = 1.5 and 2.0, and q_o = 1.2 and 1.0, cases. As far as the calculations are limited within the above

class of MHD equilibrium, the maximum critical beta value of about 3% is reached for the $\beta_J = 1.5$ and $q_o = 1.2$ case.

If we neglect the results from the Mercier criterion and the q_o value of as low as unity is possible the critical value is improved considerably, especially, for the $\beta_J = 1.5$ case ($\bar{\beta}_t \simeq 5\%$). Even in this case, however, the beta value for $\beta_J = 2.0$ case is less than 3%.

In conclusion it seems possible to increase the critical beta value above ~4% by considering wider range of equilibrium classes with fairly low $\bar{\beta}_p$ and q_b values and introducing higher order deformation of magnetic surfaces.

3.1.2 High ballooning mode instabilities

In this subsection we study the dependence of the critical beta value ($\bar{\beta}_t$) on the poloidal beta value (β_p) for various classes equilibria and look for stable equilibria with higher beta values. First we show the dependence of $\bar{\beta}_t$ on the toroidal mode number (n) for the equilibrium (Eqs.(3-2)-(3-4) (Fig. 3-3) where the conducting wall is placed at $\Lambda = 1.2$ (Λ=b/a, b: radius of the conducting wall, a: plasma minor radius). The critical beta values for n = 1, 2 and n = ∞ are obtained by using the ERATO code and ballooning stability code (BOREAS), respectively. It is easily understood from this figure that the ballooning criterion gives the sufficient stability condition (lower bound of $\bar{\beta}_t$).

In this way, often it is safe to use the ballooning criterion as the sufficient stability criterion for the linear ideal MHD modes. Therefore in the following parameter survey, we only take into account the ballooning criterion to obtain the possible maximum beta value.

The classes of equilibria which were investigated are,

Class 1: Eq. (3-2)

$$\text{Class 2: } p(\psi) = \left(\frac{\psi-\psi_b}{\psi_m-\psi_b}\right)^{\alpha}, \quad T\frac{dT}{d\psi} = R_o^2\,(1/\beta_J-1)\frac{dp}{d\psi}, \tag{3-5}$$

$$\text{Class 3: } p(\psi) = \frac{\alpha_1}{2}\psi^2 - \frac{\alpha_2}{3}\psi^3, \quad T\frac{dT}{d\psi} = \alpha_2 R_o^2\psi^2 + \alpha_4\psi^4 \tag{3-6}$$

The results are summarized as the dependence of $\bar{\beta}_t$ on β_p in Fig. 3-4. From this figure we conclude that $\bar{\beta}_t \gtrsim 4\%$ for $\beta_p = 1.5$ and $\delta = 0.2$ is attainable, where δ denotes the triangularity. In the limit of $n = \infty$ the MHD approximation is suspicious and the correction of the finite-n effect is expected to be favorable on $\bar{\beta}_t$. We can, therefore, expect that $\bar{\beta}_t \gtrsim$ 5-6 % is attainable for the parameters of the INTOR.

3.1.3 Summary on theoretical β-limit

As for stability of linear ideal MHD modes the following, generally, hold,

(1) The n=1 external kink mode is completely stabilized by a closely located conducting wall. As this mode is difficult to stabilize by an active feedback system, it should be stabilized by locating the conductive wall close to the plasma.

(2) In the case of equilibria with $TT' \propto p'$ which are usually adopted for numerical analyses, higher beta value is attained by lowering poloidal beta value and safety factor at the plasma surface (q_a). It is possible that some other sophisticated equilibria may give higher beta value for higher poloidal beta value. What kinds of equilibria among them are realizable depends on transport processes and this problem will be solved by using 1-1/2D(2D) tokamak codes.

(3) As for the shape of plasma boundary triangularity improves the stability property and raises beta value considerably.

References

1) R. Gruber, R. Schreiber, F. Troyon, W. Kerner, K. Lackner, A. Sykes, and J.A. Wesson, "Dependence of Ideal MHD Beta Limits on Current Density and Pressure Profiles", Seventh International Conference on Plasma Physics and Controlled Nuclear Fusion Research Innsbruck 23-30 August, 1978 IAEA-CN-37/K2.

2) Y-K.M. Peng, R.A. Dory, D.B. Nelson, and R.O. Sayer, Phys. Fluids 21 (1978) 467.

3) D. Berger, L.C. Bernard, R. Gruber, and F. Troyon, "Wall Stabilization Action on MHD Instabilities", ORNL-TM-6219 (April 1978).

4) T. Tsunematsu, T. Takeda, G. Kurita, T. Matsuura, and R. Gruber, "The Stabilizing Effects of a Conducting Shell on MHD Instabilities",

in preparation.

5) D. Berger, "Numerical Computations of the Ideal Magnetohydrodynamic Stability of Small Aspect Ratio Tokamaks", LRP 131/77 (September 1977).

Table 3.1 Parameters for the analyses of the beta limit of the INTOR

Aspect ratio (A)	4.0	
Ellipticity (E)	1.5	
Approximate Poloidal Beta (β_J)	1.5	2.0
Toroidal Mode Number (n)	1 and 2	1 and 2
Safety Factor at the Magnetic Axis (q_o)	~1.0 and ~1.2	~1.0 and ~1.2

Table 3.2 Summary of the analyses of the beta limit

$\beta_J(\sim\bar{\beta}_p)$	$q_o = 1.2$		$q_o = 1.0$	
	n = 2	n = 1	n = 2	n = 1
2.0 (2.00)	$q_b = 4.6$ $\bar{\beta}_t = 1.85\%$	$q_b \leq 3.7$ $\bar{\beta}_t \geq 2.26\%$	$q_b = 3.68$ $\bar{\beta}_t = 2.84\%$	$q_b = 3.68$ $\bar{\beta}_t = 2.84\%$
	$\bar{\beta}_t = 1.85\%$		$\bar{\beta}_t = 2.84\%$	
1.5 (1.42)	$q_b = 2.65$ $\bar{\beta}_t = 3.00\%$		$q_b = 2.0$ $\bar{\beta}_t = 5.2\%$	$q_b = 2.1$ $\bar{\beta}_t \geq 4.56\%$
	$\bar{\beta}_t = 3.00\%$		$\bar{\beta}_t = 4.56\%$	

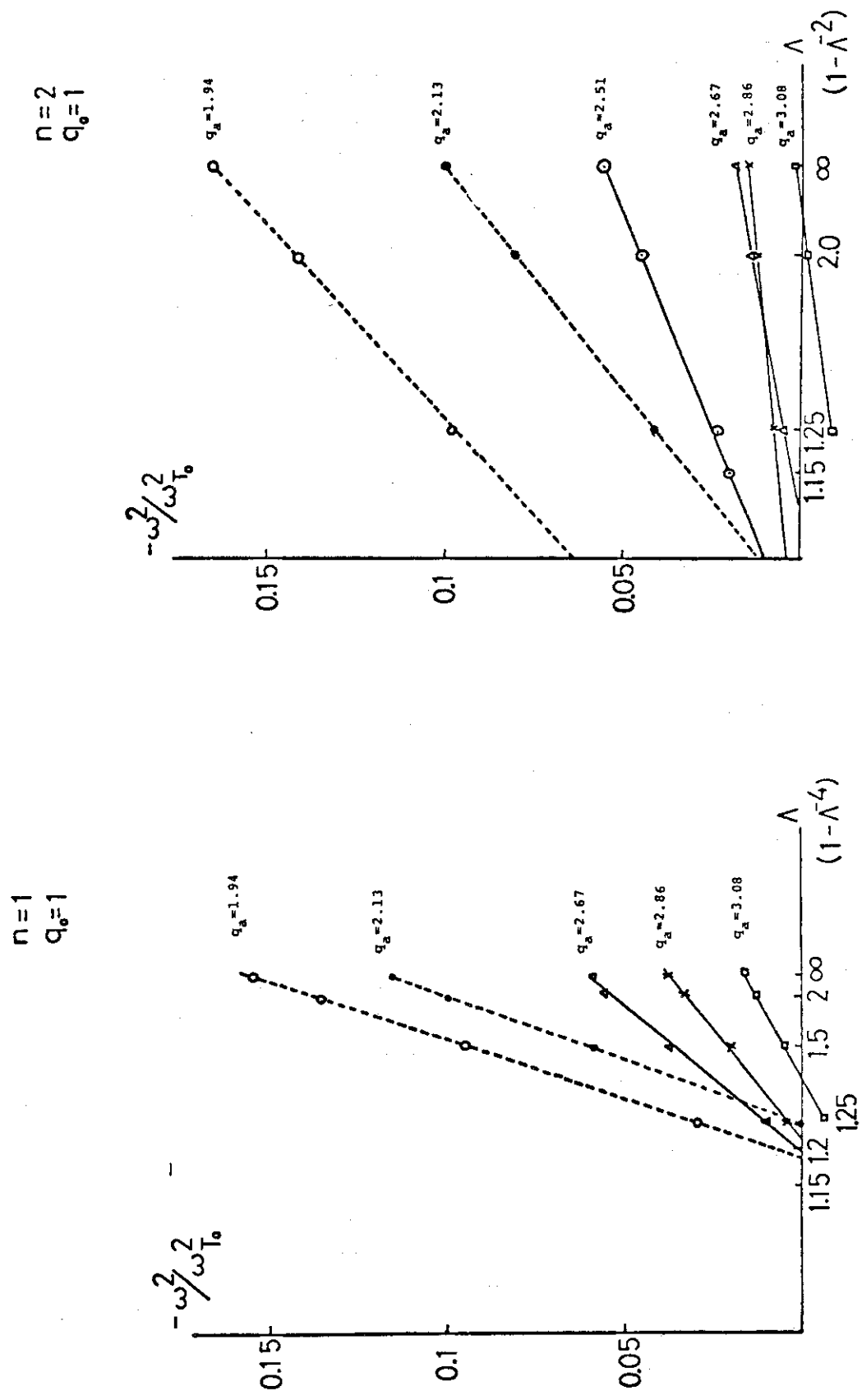

Fig. 3.1 Effect of conducting wall for a circular cross-section tokamak with A=3, E=1.0, q_o = 1.0.
(a) n=1 mode instability (b) n=2 mode instability

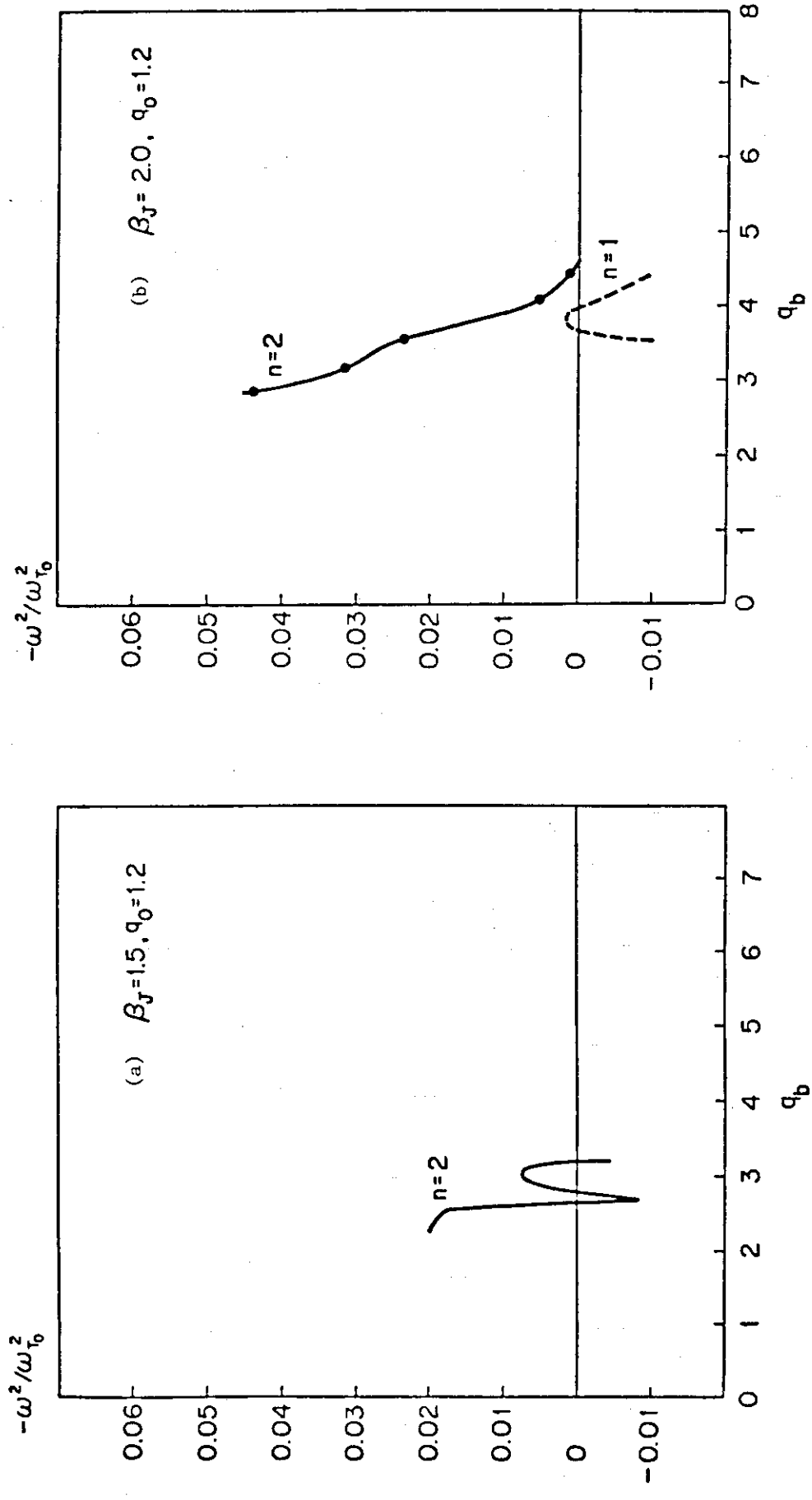

Fig. 3.2 Normalized growth rate versus the q value at the plasma boundary (q_b)
(a) β_J=1.5 sec (b) β_J=2.0 case

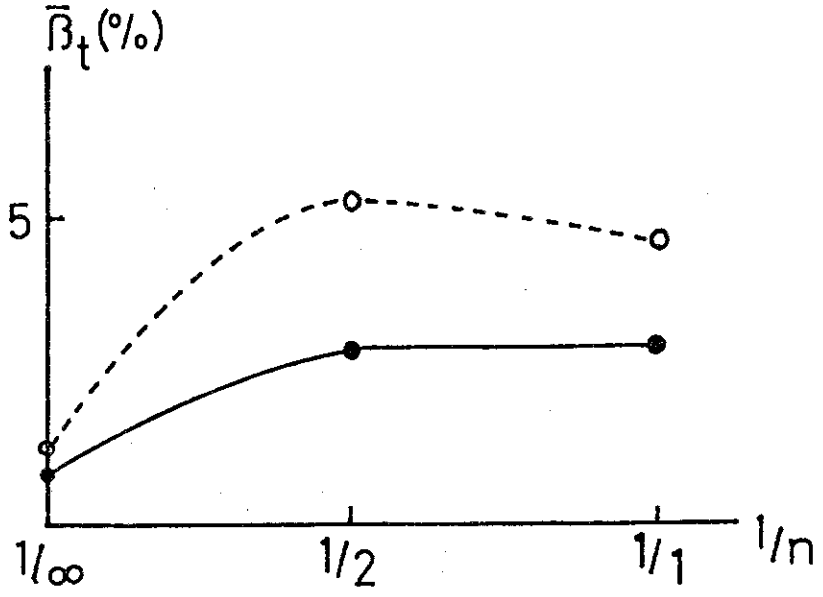

Fig. 3.3 The critical beta value versus the toroidal mode number for β_p=1.5(dashed line) and β_p=2.0(solid line). Conducting wall is placed at Λ=1.2.

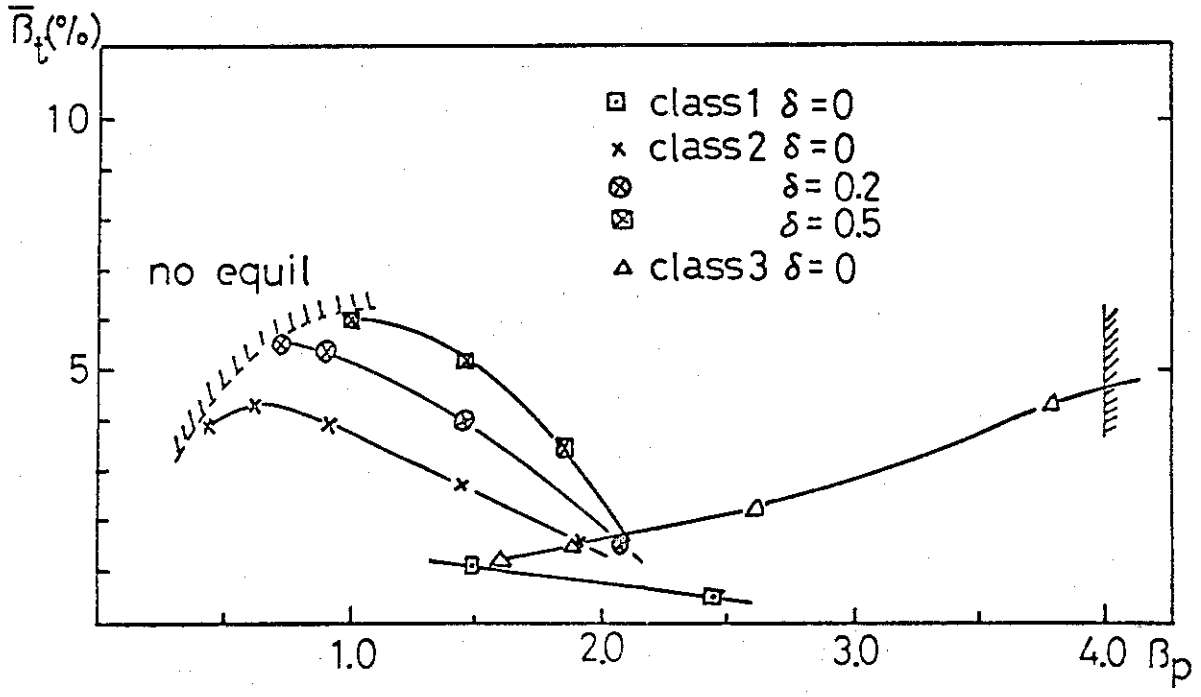

Fig. 3.4 The critical beta value versus the poloidal beta value. In the shaded region at the right hand side reversed current appears in the equilibrium current profile.

3.2 Experimental program under way to investigate β-limit

See Table 3.3.

Table 3.3 Experimental program under way to investigate the β limit

	JFT-2	JFT-2M (1981)		JT-60 (1983)
$\tau_{heating}$ (s)	0.05	0.1 ∿ 0.2		5 ∿ 10
divertor	NO	NO		YES
R (m)	0.9	1.25		3
a (m)	0.25	0.3		0.95
b/a	1	1.6		1
B_t (T)	1.6	1.5	4.5 (1984)	4.5
I_p (MA)	0.16	0.3	1.0	2.7
NBI (MW)	1.5 (1979)	5	≥ 10	15 (1984), 30 (1985)
ICRF (MW)	1 (1980)	1		
LHRH (MW)	1 (1980)	1		1.25 (1984), 10 (1985)
$\bar{\beta}_t$ (%)	∿ 2	3 ∿ 6		2 ∿ 4

4. Disruptions and Their Consequences

4.1 Origin of major disruption and its suppression[1)2)]

After reducing impurities, no major disruption is observed in DIVA. In order to observe the disruptive instability, neon gas is injected into a stable discharge with $q_a \lesssim 2.5$. The radiation loss increases and the disruptive instability is excited with good reproducibility. Various types of precursor oscillations of m=2/n=1 are observed, e.g. simply growing fluctuations or small fluctuations followed by sudden growth. Figure 4.1 shows events immediately before and during a typical disruption. About 100 μs before the negative spike, MHD activity gradually increases, and X-ray signal from central chord decreases and from outer chord increases slowly. This means a spread of a current channel. The events in this phase are similar to those of minor and/or internal disruption. Then m=2/n=1 mode suddenly grows up to 5∿8% within 30 μs, and loop voltage drops steeply, i.e. the major disruption appears. The signal in outer chord rapidly increases, which means rapid spread of the hot column. The radiation loss including charge exchange loss is 40 kW before the neon injection and increases gradually up to 250 kW at the negative spike.

These experimental results are well simulated by combining a transport code to a tearing code. In the calculation, the initial profiles of temperature and density are given from the experimental results. Time development of the radiation loss profile and sawtooth oscillations are also given from the experimental data but other profiles are calculated by the transport code. Saturated level of the m=2/n=1 mode is calculated at any time by the tearing code. Only with the impurity injection or only with internal disruptions, the amplitude of the m=2/n=1 mode is less than 1%. However, with the impurity injection and the internal disruption, the fluctuation level is several % which is observed in the experiment. Therefore, the major disruption is induced by the impurity increase and the internal disruptions which enhance the m=2/n-1 mode.

It should be noted that the amount of neon injected to induce the disruption in the case with a divertor is 3 times larger than that without the divertor but the separatrix does not affect the major disruption as shown in a previous experiment[3)].

In DIVA, a discharge in $q_a < 2$ region has been stably obtained by reducing a radiation loss. Examples of the discharge are shown in Fig. 4.2. When the plasma current is crossing through $q_a = 2$, m=2/m=1 which may be surface mode grows up to $\tilde{B}_p/B_p = 4\%$ and the loop voltage rises, but negative voltage spike is not usually observed. The characteristic feature of the MHD activity is not changed by changing the current rising time from 2.5 to 6 ms. When the plasma has a separatrix in the shell, duration of voltage increase is shorter than the case without the separatrix, and the MHD activity is much smaller than that without the separatrix by a factor of 4. Therefore the separatrix stabilizes the surface mode. When the discharge fall into $q_a < 2$ region, fluctuations including m=3/n=2 are observed by magnetic probes but the level is very low, i.e. $\tilde{B}_p/B_p = 0.05\%$.

Large sawtooth oscillations are observed in soft X-ray signal and loop voltage, and the energy confinement time τ_E is dominated by these internal disruptions in very low-q discharges. The average energy confinement time, however, follows Alcator scaling with a higher numerical factor in front of $\bar{a}^2 n_e q_a^{1/2}$.[2)4)]

Examples of neon injection into the stable $q_a < 2$ discharge is shown in Fig. 4.3. It should be noted that no major disruption occurs in $q_a < 2$ region which is contrast with disruption in $q_a > 2$ region. When neon gas is injected into a stable $q_a = 1.6$ discharge, the loop voltage increases as increasing radiation loss, and because of increasing resistivity the plasma current decreases. After the safety factor q_a becomes larger than two, the major disruption occurs.

The number of observed disruptions at different q_a values is plotted in Fig. 4.4. It can be clearly seen that the disruptive instability does not appear in $q_a < 2$ region. This result is consistent with the conclusion that the origin of the disruption is m=2/n=1 internal mode. The major disruption is easily suppressed by reducing impurity level. If the impurity efflux from the first wall is serious, the separatrix magnetic surface reduces the impurity effect as discussed before and may suppress the major disruption. If the internal disruption is suppressed, the major disruption can be suppressed.

References

1) K. Odajima, M. Nagami, S. Yamamoto et al., Symposium on Current Disruption in Toroidal Devices, Garching, IAEA (1979).
2) DIVA Group, Study on Very-Low-Q Discharges in DIVA, JAERI-M 8205 (1979).
3) Y. Shimomura et al., Phys. Fluids 19 1635 (1976).
4) H. Maeda et al., 7th International Conference on Plasma Physics and Controlled Nuclear Fusion Research (Innsbruck, 1978) paper T-3-1.

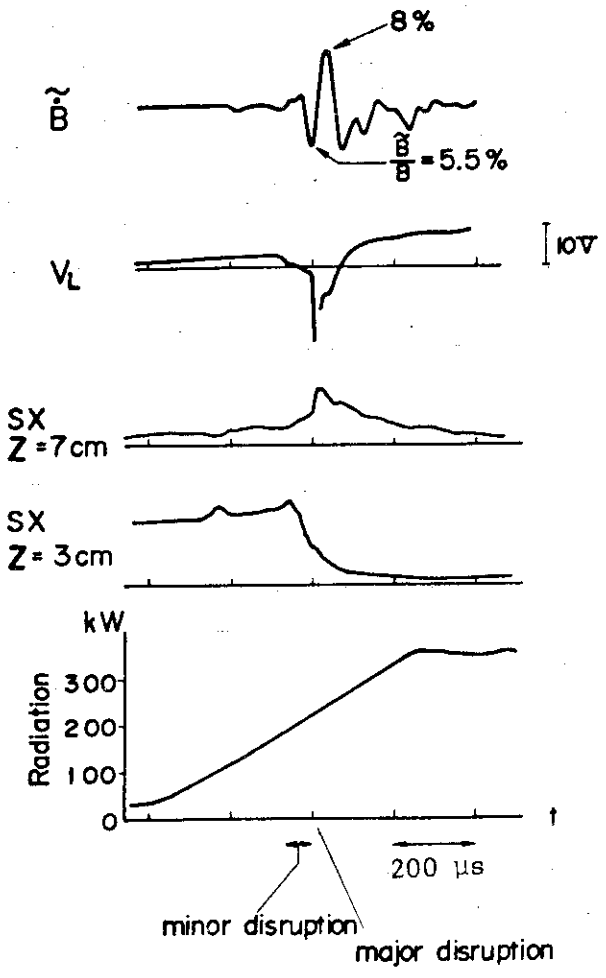

Fig.4.1 Typical example of major disruption. Neon is injected into stable q_a = 2.5 discharge at 1.5 ms before the negative spike. The disruption is separated into two steps, the first is slow decrease of V_L and the second is abrupt drop of V_L.

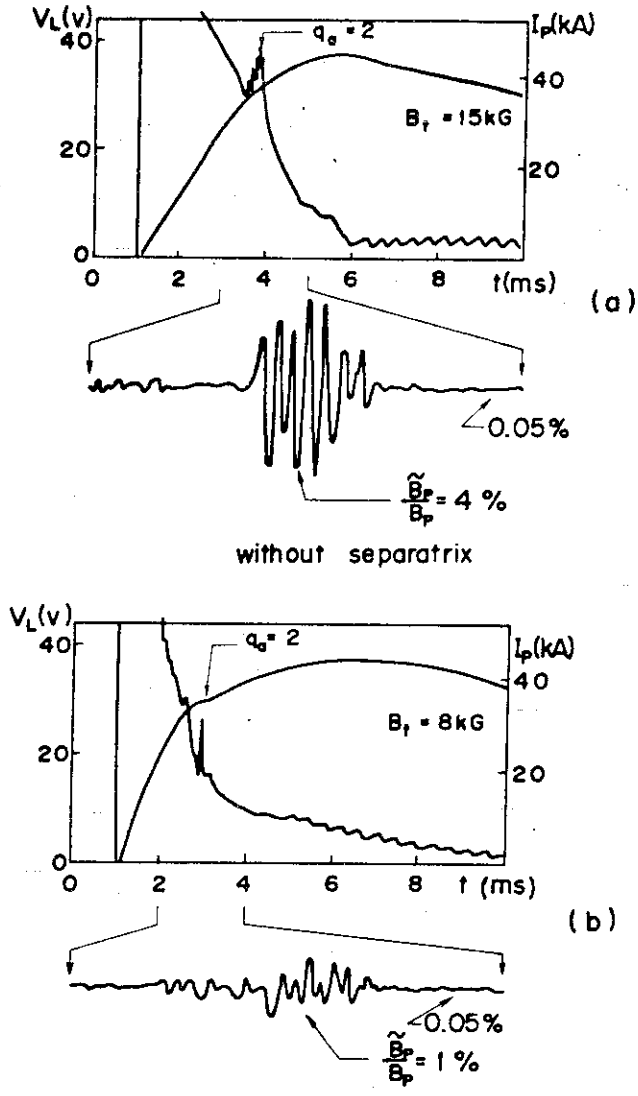

Fig.4.2 Examples of q_a < 2 discharge. (a); without separatrix (b); with separatrix. When the plasma current crossing through q_a = 2, m = 2 surface mode grows up to 1% for the case with separatrix and 4 % without. In q_a < 2 region, sawtooth oscillations are seen in loop voltage, and magnetic fluctuations including m=3/n=2 is very weak typically 0.05% in both cases.

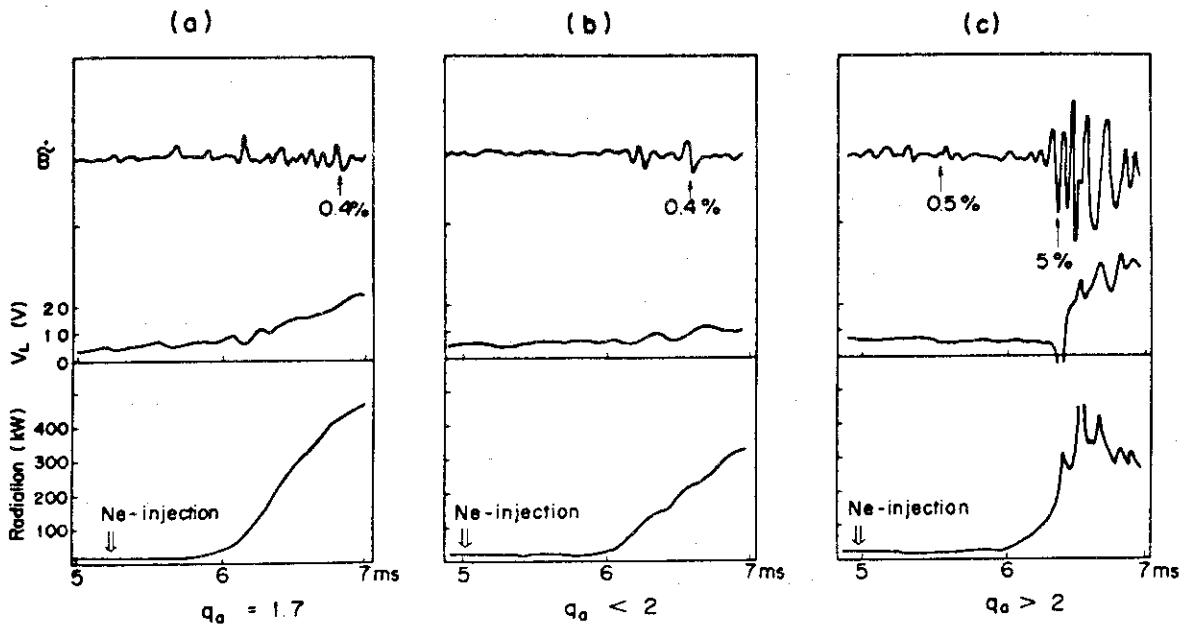

Fig. 4.3 Neon injection into q_a = 1.7 (a), and q_a is around two discharges [(b) in case q_a < 2 and (c) in case q_a > 2]. Radiation loss in all cases increases in almost the same manner, but there is no major disruption in the former two cases in contrast to the last.

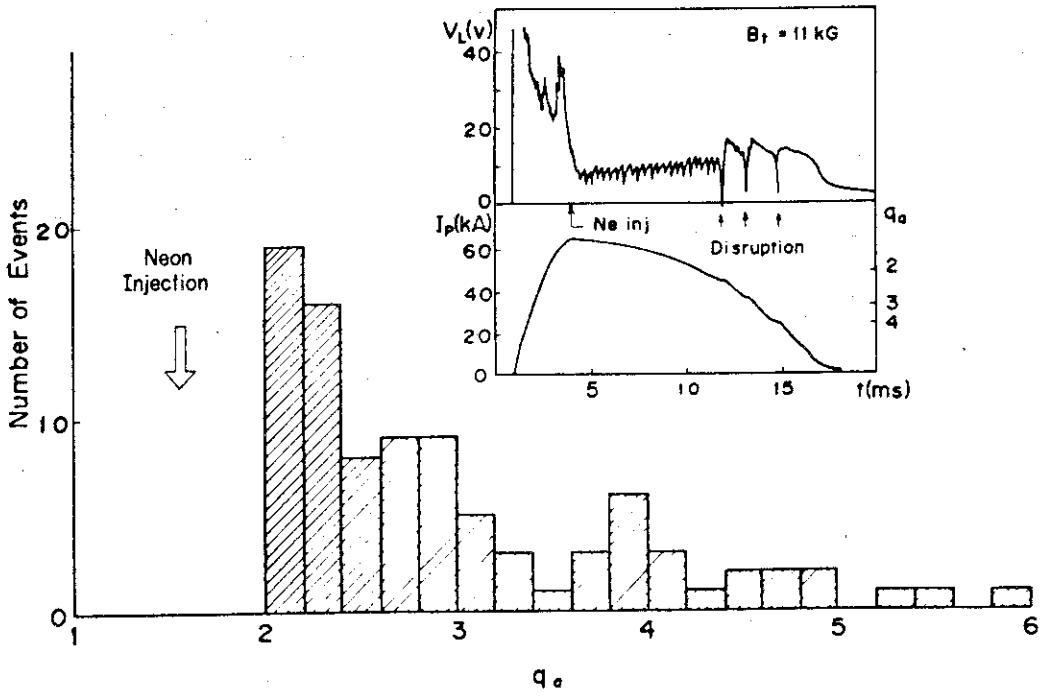

Fig. 4.4 The number of observed disruptions at different q_a, when neon gas is injected into stable q_a = 1.6 discharge. It can be clearly seen that the disruptive instability does not occur in q_a < 2 region.

4.2 Heat flux due to major disruption

The total energy loss due to the major disruption is almost equal to the plasma energy before the disruption. Therefore, around 100 Mjoule energy flows on to the first wall. The major part of the energy flows along the magnetic field lines and damages the limiter surface in a conventional tokamak.

With the divertor, the heat flux is well guided into the burial chamber even during the disruption as observed in the DIVA experiment.[1] The thickness of the scrape-off layer is controlled by the non-axisymmetric magnetic field.[2] Therefore, the heat flux due to the major disruption can be rather easily controlled in a divertor device.

References

1) Y. Shimomura et al., Phys. Fluids 19 (1976) 1635.
2) S. Yamamoto et al., Nuclear Fusion 18 (1978) 2.

4.3 Effects by minor disruptions or internal disruptions[1]

The internal disruptions as well as the minor disruptions induce the particle and heat losses to the first wall. These loss flux induces the impurity production as observed in Fig. 4.5. In a large device this effect becomes serious in a conventional device. In a divertor device, however, the losses are guided into the divertor where impurities are produced. In this case, the impurities can hardly flow into the main plasma.

Reference

1) S. Yamamoto (DIVA group), private communication.

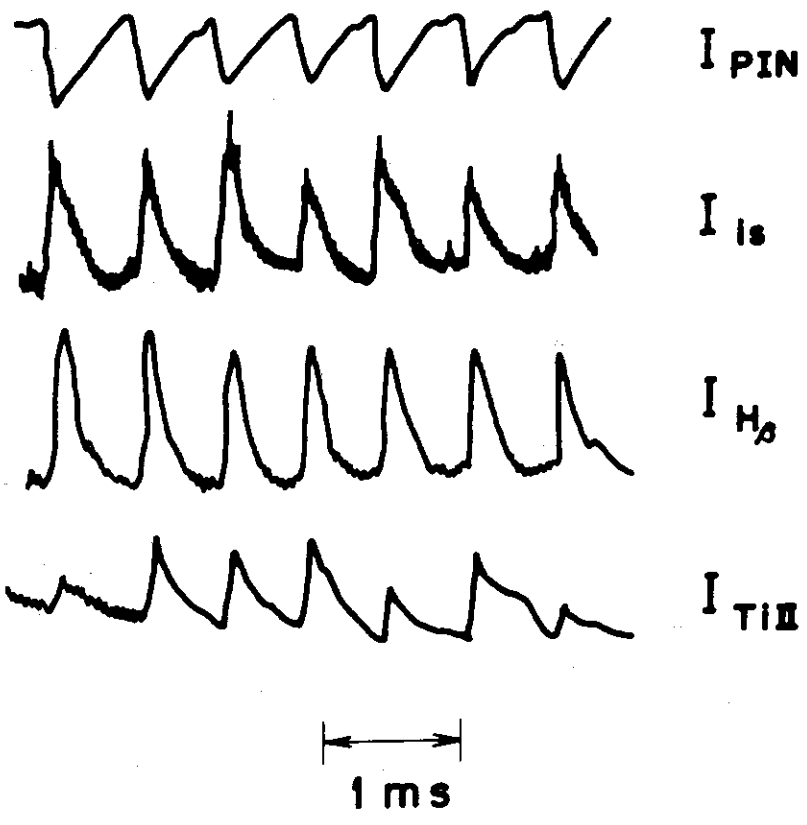

Fig. 4.5 Impurity influx due to the internal disruptions. I_{PIN}, I_{is}, $I_{H\beta}$, and I_{TiII} are intensity of X-ray, ion saturation current and intensities of H_β and TiII, respectively.

5. Stability Control

5.1 Positional instability

Stabilization of a positional instability is a very important problem for an elongated tokamak plasma. If one can locate a perfectly conducting wall close to the plasma surface the instability can be stabilized. From technological requirements, however, the distance between the plasma surface and the conducting wall is restricted above a certain value, and moreover the wall is not perfectly conducting.

First we assess the maximum permissible distance between the plasma and wall to stabilize the positional instability only by a perfectly conducting wall. Then we investigate problems on an external control system which is required to stabilize the instability when the conductivity of the wall is finite.

5.1.1 Effects of triangularity and rectangularity on positional instability

The positional instabilities (n=0 mode) are analyzed for several different shapes of plasma cross-section by the ERATO code. The growth rate of the instability is calculated by varying the plasma-wall distance (Λ=b/a) and the critical value of Λ is determined by exterpolation (Fig. 5.1). It is concluded that the plasma of the INTOR can be made stable against the positional instability by locating a perfectly conducting wall at $\Lambda \leq 1.5$, irrespective of triangularity and rectangularity.

5.1.2 Dependence of positional instability on ellipticity

In the previous subsection we showed that the INTOR plasma of elliptical cross-section with and without triangularity would be stable against n=0 axisymmetric mode for $\Lambda \lesssim 1.5$. In this subsection we examine the dependence of the positional stability on the ellipticity. The motivation of this study is to know whether the ellipticity of 1.5 is appropriate from the viewpoint of the positional instability.

Figure 5.2 shows the results of the calculation, where the growth rate of the n=0 mode vs. ellipticity is plotted for different triangularity of the plasma shape. Conclusions from this figure are summarized as follows,

i) A plasma with any ellipticity and any triangularity will be stabilized against the n=0 mode instability if a perfectly conducting

wall is located sufficiently close to the plasma surface ($\Lambda \lesssim 1.5$). This result was already obtained in the previous subsection and confirmed again for different plasma parameters (previously: $q_a \sim 2.5$, $\beta_p \sim 1.3$, present case: $q_a \sim 4.0$, $\beta_p \sim 2.0$).

ii) If there is no conducting wall which has sufficiently long skin time, plasmas with any crosssectional shape will be unstable against the n=0 mode. In this case decrease of the ellipticity does not improve the stability property of the plasma.

iii) For $\Lambda \simeq 1.6$ and $E \simeq 1.5$, the positional stability depends very sensitively on the shape of the plasma surface. The guiding parameters of the INTOR are considered to be close to the optimum ones. But it is desirable to analyze the stability more minutely.

Remaining problems which have not been studied up to now are,

i) Existence of separatrices of vacuum field is considered to deteriorate the positional stability, but it has not been studied yet as all the analyses up to now are on fixed boundary equilibrium for given plasma boundary.

ii) In our analyses it is assumed that the conducting wall completely surrounds the plasma but in the actual device the conducting wall has some slits which may deteriorate the stability. The positional stability will be worsened by taking into account this effect but it will be recovered by considering the nonlinear saturation of the mode. Anyway more detailed analyses are desired.

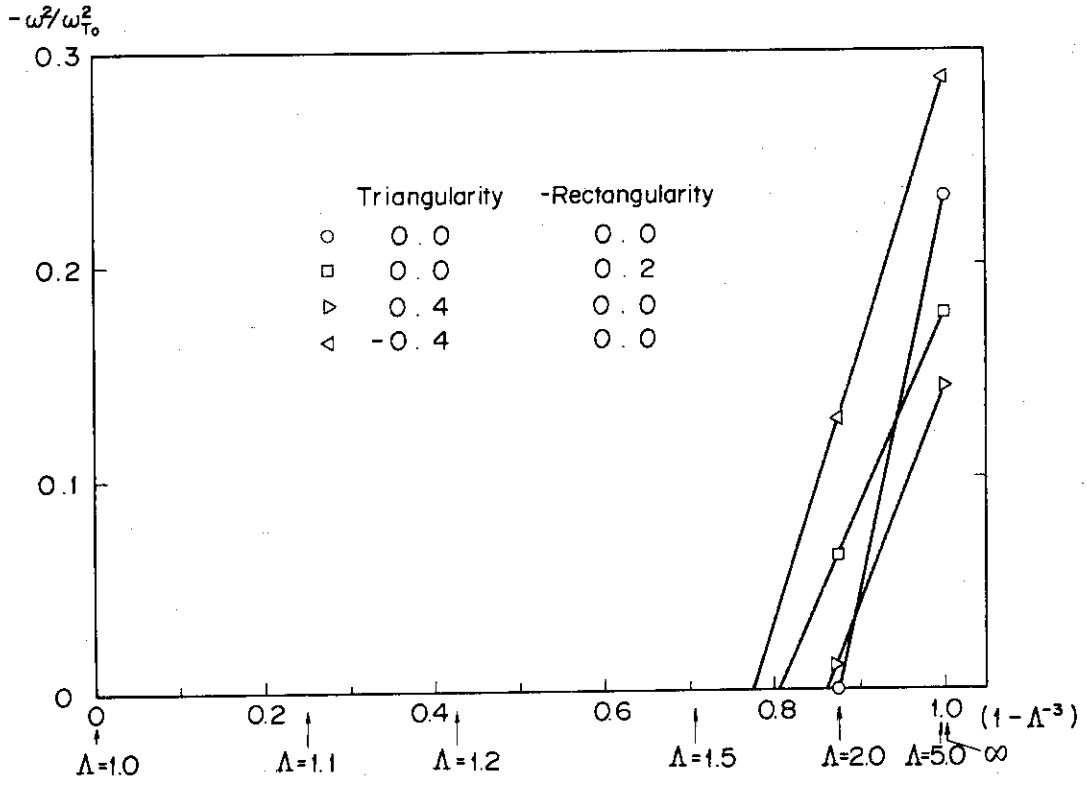

Fig. 5.1 Growth rates of positional instability vs. the position of conducting wall (Λ = b/a).

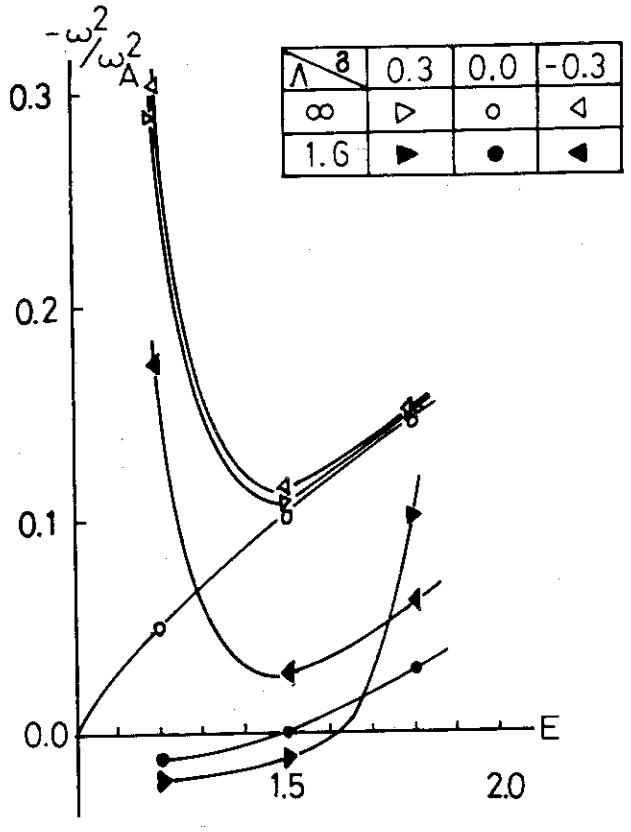

Fig. 5.2 The growth rate of the n=0 mode versus ellipticity(E). The growth rate is normalized by the toroidal Alfven frequency at the magnetic axis.

5.2 Disruption control

The major disruption induces a sudden energy loss to the first wall and the energy loss is typically 100 MJ. With the simple poloidal divertor, the energy loss are guided onto the neutralizer plate as observed in DIVA[1] and the energy loss density is about 1 MW/m^2. This value is not very high and the neutralizer plate may not be destroyed by 1000 major disruptions. Without the divertor, however, the loss energy concentrates on a small area and evaporates the first wall material seriously. Therefore, the major disruption has to be completely suppressed in an INTOR without the divertor if the limiter cannot be easily repaired.

Energy loss due to internal disruption is usually small in a high q discharge, but is large in a low-q discharge planned in INTOR. In DIVA, the energy loss is 10 % or more of the total plasma energy (Fig. 5.3). In INTOR, the loss energy is estimated to be about 10 MJ assuming $a_{q=1} = \frac{1}{2} a_p$ during 0.3 sec with $\chi_e = 5 \times 10^{19}/n_e \ m^2/sec$ at $q > 1$. Therefore it is necessary to spread the energy loss to a wide area, typically 10 m^2. Without the divertor, the energy loss may concentrate on a small area. From this point of view, the internal disruption has to be usually suppressed in an INTOR without the divertor.

Origin of major disruptions in a low-q discharge planned in INTOR is mainly large m=2/n=1 fluctuations which are induced by impurity injection and internal disruption as observed in DIVA experiment and in the numerical simulation[3]. Therefore the major disruption is completely suppressed if the m=2/n=1 fluctuations are stabilized.

In a $q_a < 2$ discharge, there is no resonance surface of m=2/n=1 and the major disruption is completely suppressed as shown in Fig. 5.4. The $q_a < 2$ discharge was easily obtained in DIVA having a close shell ($a_s/a_p \leq 1.3$) with the following first wall material[3),4)].

a) Clean Au wall with the divertor

b) Clean Ti wall or clean C wall with and without the divertor (Fig. 5.5)

Therefore it is easy to obtain the $q_a < 2$ discharge in an INTOR with a SS blanket. In an INTOR with a reasonable tritium breeding blanket, the close shell effect cannot be expected and the stable $q_a < 2$ discharge cannot be obtained.

The other method to stabilize m=2/n=1 mode is to obtain a stable profile for the mode. The m=2/n=1 mode is unstable in a special profile

which is usually obtained by impurity injection and internal disruption. Therefore it is easy to obtain a stable profile for the m=2/n=1 mode especially in a device having a local heating method (e.g. ICRF heating as shown in Fig. 5.6). The stable profile, however, changes to an unstable profile by impurity injection and internal disruption in the present tokamak. In a high temperature plasma, the internal disruption may be suppressed during 100-200 sec and the large impurity influx can be suppressed with the simple poloidal divertor. Therefore the major disruption is normally suppressed. The other modes, e.g. ballooning mode, have a possibility of flattening the profile near the axis and a sudden impurity influx may occur without the divertor. In this case, some control methods are required.

Concerning internal disruption, the time constant of current penetration, however, is very long in INTOR and 50 sec. is necessary to reduce q_o from 1 to 0.8, i.e. if the initial q_o of 1.6 is obtained the internal disruption does not occur during the duration. Therefore a local heating method is also required to control the initial q profile.

Active control os the disruption has not been demonstrated and it seems very difficult. Therefore it is reasonable to consider that the m=2/n=1 mode cannot be actively controlled. From this point of view the profile control is more realistic as discussed before. A profile tending to the unstable one for the m=2/n=1 mode or the precursor oscillations can be detectable. Changing the profile with a local heating and a local cooling, the major disruption can be suppressed.

References

1) Y. Shimomura et al., Phys. Fluids 19 (1976) 1635.
2) DIVA group, Study on Very-Low-q Discharges in DIVA, JAERI-M 8205 (1979).
3) K. Odajima et al., Symposium on Current Disruption in Toroidal Devices, Garching, IAEA (1979).
4) S. Sengoku, T. Matsuda, H. Matsumoto et al., private communication.
5) H. Kimura, K. Odajima et al., private communication.

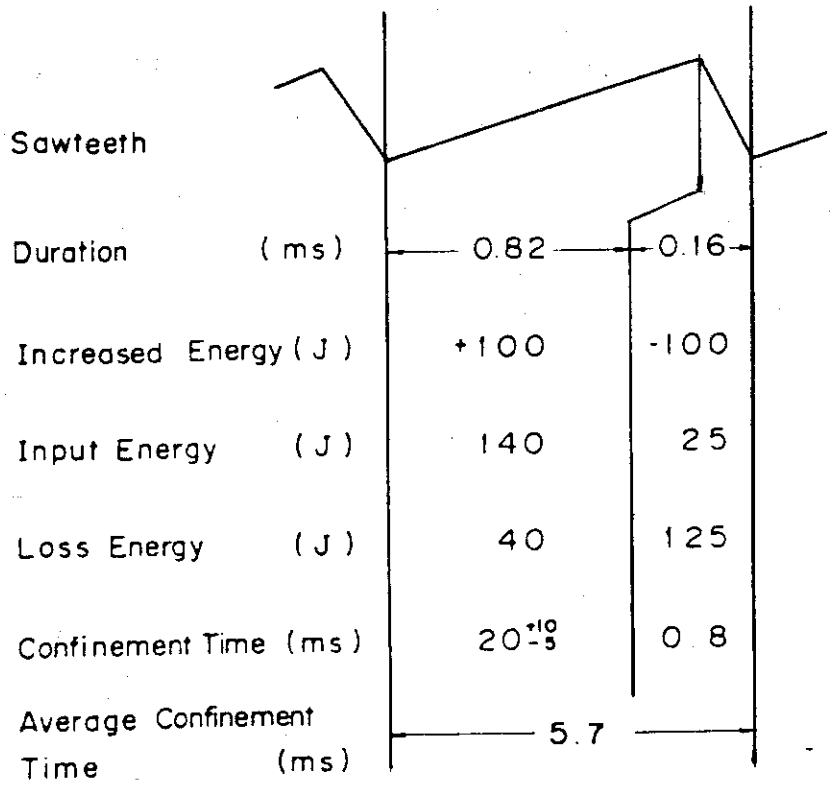

Fig. 5.3 Energy balance in a sawtooth oscillation.[2)]

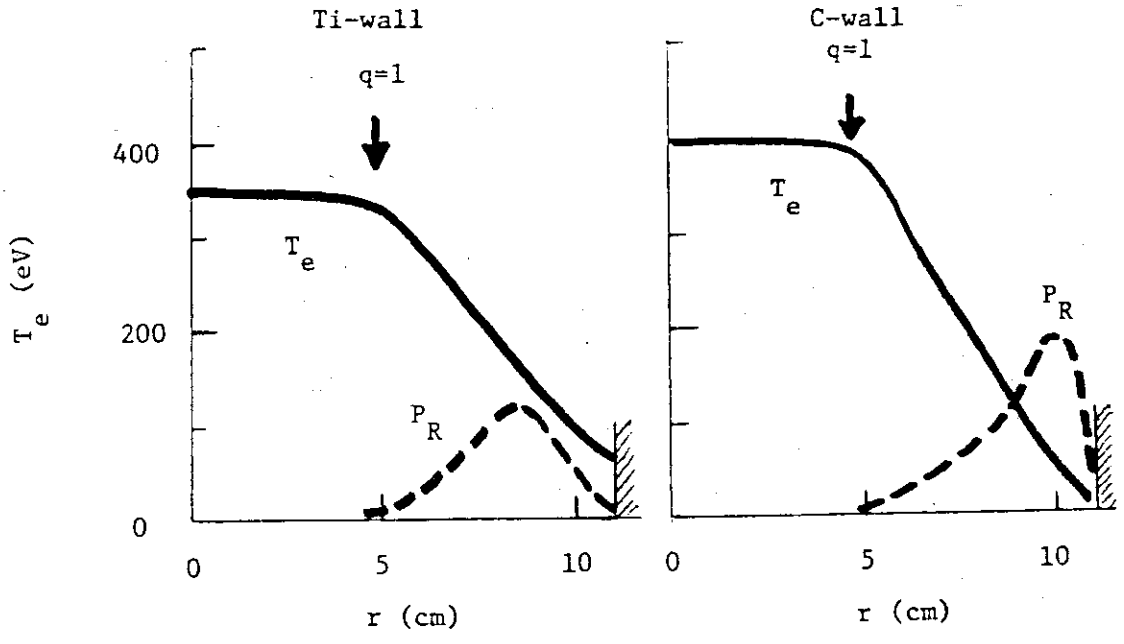

Fig. 5.5 Very low q discharges with C-wall and T_i-wall at $q_a \sim 1.9$. $n_{e0} = 7\times10^{13}$cm^{-3}, τ_E=3.2 ms, radiation loss $P_R \approx (15\sim20)$% of imput power and $Z_{eff} \lesssim 1.5$ with T_i-wall. $n_{e0} = 5\times10^{13}$cm^{-3}, τ_E = 2.8ms, $P_R \approx 30$% and $Z_{eff} \lesssim 2.0$ with carbon wall.

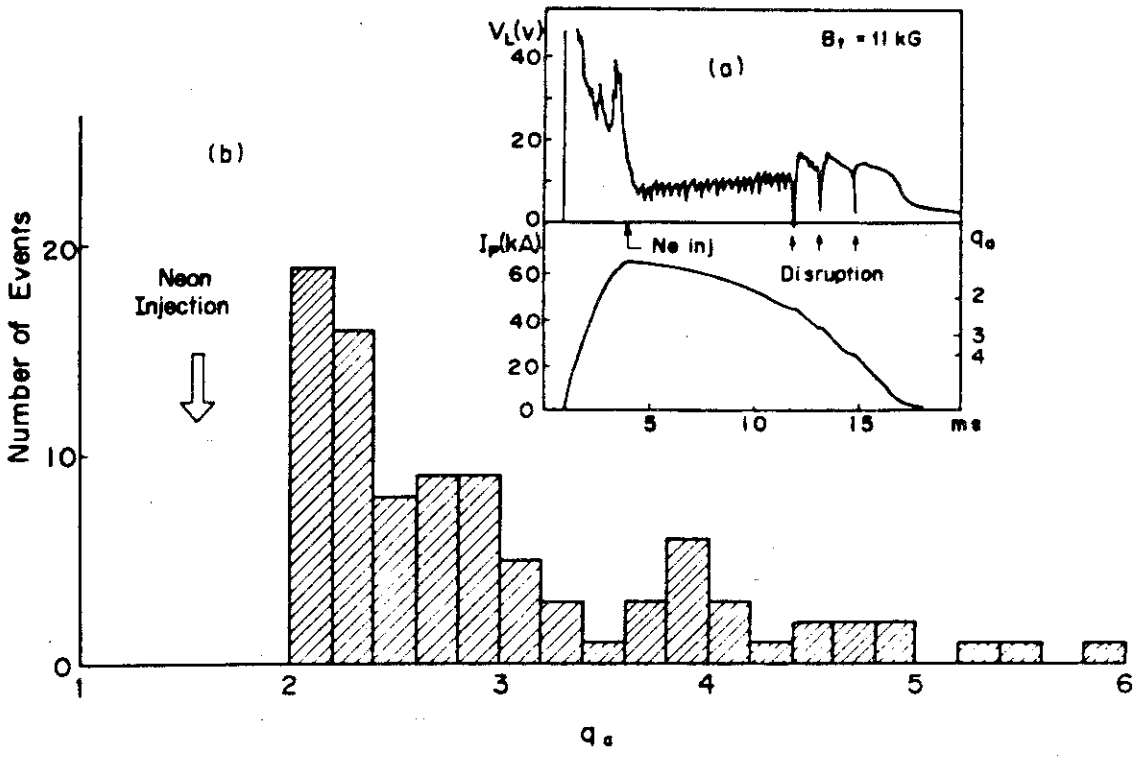

Fig. 5.4 Typical plasma parameters and number of occurrence of observed disruptions at different q_a when the neon is injected into the stable q_a=1.6 discharge.
Major disruptions do not occur when the safety factor q is less than 2.[3)]

(a) Time behavior of loop voltage and plasma current with neon injection at 4 ms into the stable q_a = 1.6 discharge. The loop voltage increases at increasing radiation loss, and the plasma current decreases due to increasing resistivity. After the safety factor q_a becomes larger than two, the first major disruption occurs, and a series of voltage spikes appears on the loop voltage.

(b) The number of occurrence of observed disruption at different q_a.
Disruptions are frequently observed near q_a = 2.

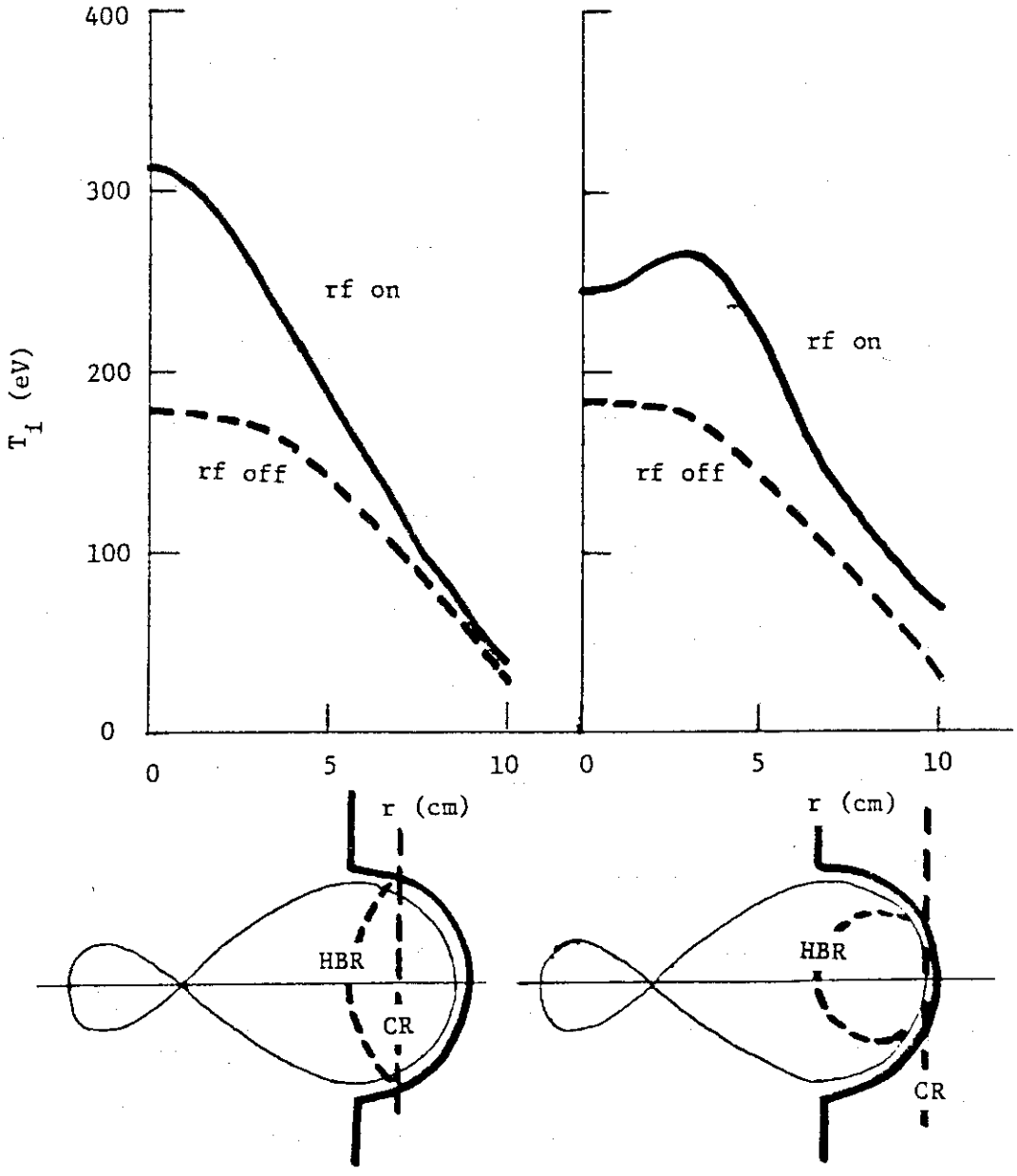

Fig. 5.6 Local heating by ICRF in a hydrogen minority plasma. HBR : hybrid resonance layer. CR : cyclotron resonance layer for hydrogen.[4)]

5.3 Profile control

As described in the previous sections we must carefully realize an appropriate stable MHD equilibrium in order to reach a higher beta state. For this purpose some kinds of profile control may be required. In the following we discuss qualitatively some possible methods of profile control.

Density profile control will be done by the gas and pellet injection techniques which are extensions of a present method used for total density control. Current profile control during the current build-up phase may be done by expanding the plasma minor radius[1,2]. This technique is still to be developed and the profile will be controlled by combining several methods, for example, the gas injection and heating of plasma periphery by RF heating.

As the profile control of the density, current, etc. interacts each other, it is useful to introduce the modern control theory. The first necessary step in the control strategy is to construct the mathematical model of the control object being studied. Once a mathematical model is constructed, it is easy to obtain the so-called state equation of linear dynamical system and to adopt the modern control theory. There are two methods to construct the mathematical model:

(a) Mathematical model on the bases of the application of basic physical laws, i.e., Newton's laws, Maxwell's laws, mass balance, energy/heat balance, etc.,[3]

(b) Mathematical model on the bases of the application of identification method.

Preliminary applications of these two methods for current profile control is being studied now.

References

1) T. Kobayashi, T. Tazima, K. Tani and S. Tamura : JAERI-M 7014 (1977).

2) H. Ninomiya, A. Kameari and Y. Suzuki : JAERI-M 6656 (1976).

3) A. Ogata and H. Ninomiya : Jpn. J. Appl. Phys. 18 (1979) 825.

5.4 Feedback control system and shell effect of SS blanket

5.4.1 Block diagram of the control system

First, we derive the block diagram of the control system for the vertical position. From the equation of the vertical plasma motion, we obtain the relation between the vertical displacement Z and the magnetic field disturbance B_d as follows[1];

$$F(s) = \frac{Z(s)}{B_d(s)} = - \frac{R_p/B_{v0}}{s^2\tau_0^2+n} , \tag{5-1}$$

where the rigid motion of plasma is assumed. (The list of symbols are given at the end of this section.)

The eddy current induced in the shielding material stabilizes the plasma motion and this shell effect is represented as[2]

$$I_i(s) = - \left.\frac{\partial M_{pi}}{\partial Z}\right|_{Z=0} \frac{I_p}{L_i} \frac{s\tau_i}{1+s\tau_i} Z(s), \tag{5-2}$$

$$B_{hi}(s) = \nu_i I_i(s) .$$

The current of the feedback control loop is in proportion to Z as follows;

$$I_c(s) = G_c(s) \frac{1/R_c}{1+s\tau_c} Z(s) . \tag{5-3}$$

The eddy current is also induced by the time variation of the feedback control loop current, so the field due to the feedback control loop is

$$B_{hc}(s) = \left(\nu_c - \nu_i \frac{M_{ci}}{L_i} \right) \frac{s\tau_i}{1+s\tau_i} \cdot \frac{1/R_c}{1+s\tau_c} \cdot Z(s) . \tag{5-4}$$

The induced voltage by the plasma motion and the eddy current variation also occurs in the feedback control loop, but, in this case, we neglect this shell effect of the feedback control loop, because the position of the feedback control loop is out of the toroidal coil. From eqs. (5-1) - (5-4), we can obtain the block diagram of the control system for vertical position as shown in Fig. 5.7

The relation between Z and B_d including the effect of the eddy current and the feedback control loop becomes

$$F(s) = \frac{Z(s)}{B_d(s)} = -\frac{R_p/B_{v0}}{s^2\tau_0^2 + [n + n_i \frac{s\tau_i}{1+s\tau_i} + N_c(s)]} \quad , \tag{5-5}$$

where

$$n_i = -\nu_i \frac{\partial M_{pi}}{\partial Z} \frac{I_p R_p}{L_i B_{v0}} \quad , \tag{5-6}$$

$$N_c(S) = \nu_c \left[1 - \frac{\nu_i M_{ci}}{\nu_c L_i} \frac{s\tau_i}{1+s\tau_i} \right] \frac{1/R_c}{1+s\tau_c} G_c(s) \frac{R_p}{B_{v0}} \tag{5-7}$$

The growth rate of the vertical positional instability γ_g is given by the positive real part in poles of F(s) and following results are generally obtained.

(a) $n + n_i < 0$

No shell effect of the shielding material is expected and $\gamma_g \simeq \tau_0 \simeq 10^{-6}$sec. Thus, the feedback control of the instability is very difficult in the present technical level.

(b) $n + n_i > 0$

The shell effect of the shielding material is valid and $\gamma_g \simeq \tau_i^{-1}$. The growth rate γ_g becomes small if the gain of the feedback loop becomes large.

(c) $n + N_c(0) > 0$

This is the necessary condition for stability when $s\tau_i = 0$.

We must design the shape and the conductivity of the shielding material and the feedback control loop satisfying above (b) and (c) conditions.

5.4.2 Eddy current analysis of a SS blanket

In the present design of INTOR, a SS blanket shown in Fig. 5.8 is proposed. It consists of 6 blanket modules and each module can be divided into 4 blanket rings with the thickness of 30cm. It is easily expected that this SS blanket has a large shell effect.

First, we analyze the decay time constant of the eddy current induced in the SS blanket. The analysis is made using the finite element circuit method[3]. In this method, we introduce the current potential to solve the eddy current problem in thin conductor of any shape because the eddy current density is divergence-free. A thin conductor is subdivided into finite elements on each of which a current potential is defined. Each element is regarded to compose a electric

circuit and is coupled each other through mutual inductance and resistance matrices. A set of circuit equations which govern the time variation of the eddy current is formulated with these matrices and solved by the eigenvalue analysis.

The current distribution represented by the n-th eigenvector is called that of the n-th eigenmode. The eigenmodes are not coupled each other and the decay time constant of the n-th eigenmode is expressed by its eigenvalue. The eddy current distribution is represented by the summation of eigenvectors.

Eigenmodes by the vertical motion of plasma are different from those by the horizontal motion of plasma. In the case of the vertical motion, the eddy current flows dissymmetric about the mid-plane and produces the horizontal field. On the other hand, it flows symmetric about the mid-plane and produces the vertical field in the latter case.

Figure 5.9 shows the decay time constant and the current distribution of eddy current of the first five eigenmodes induced by the vertical motion of plasma. The model of the SS blanket is shown in Fig. 5.10 and it is assumed that there is a cut between the blanket rings. The maximum decay time constant is 751 msec and it is expected that the SS blanket has a large shell effect. This is shown in next section.

5.4.3 Shell effect of the SS blanket

It is shown in section 1 that the shell effect of the shielding material is represented by eq. (5-5). In the former session, we obtained the eddy current as the form of the eigenmodes. As mentioned previously, the eigenmodes are not coupled each other. Thus, we obtain next new characteristic equation:

$$s^2\tau_0^2 + \left[n + \sum_{i=1}^{n} n_i \frac{s\tau_i}{1+s\tau_i} + N_c(s)\right] = 0 \ , \tag{5-8}$$

$$N_c(s) = \nu_c \left(1 - \sum_{i=1}^{n} \frac{\nu_i M_{ci}}{\nu_c L_i} \frac{s\tau_i}{1+s\tau_i} \right) \frac{1/R_c}{1+s\tau_c} G_c(s) \frac{R_p}{B_{v0}} \ . \tag{5-9}$$

The growth rate of the vertical instability with no feedback is shown in Fig. 5.11. The growth rate becomes τ_i^{-1} near n = -8 owing to the shell effect of the SS blanket. Thus, the time constant about 0.7 ∿ 1.0 sec of the feedback control system is sufficient in an INTOR with the SS blanket (Fig. 5.12). The shell effect of this blanket is also available

to reduce other MHD instabilities.

However, if a reasonable tritium breeding blanket is proposed, the shell effect of the blanket will be largely reduced. For example, if the thickness of the blanket wall is 1 cm, the decay time constant becomes about several msec and we cannot expect the shell effect any more.

The detailed investigation of the shell effect of the outer shielding material has not been made yet. It is, however, expected that the outer shielding material has the decay time constant of several hundred msec, because it is the SS plate of 30 ∿ 50 cm thickness.

Symbols

R_p Plasma major radius

I_p Plasma current

m_p Plasma mass

n Decay index

B_{v0} Vertical field at R_p

L_i Self inductance of the eddy current

M_{pi} Mutual inductance of plasma and the eddy current

τ_i Decay time constant of the eddy current

n_i Decay index produced by the eddy current

ν_i Conversion coefficient of the eddy current to the horizontal field

L_c Self inductance of the feedback control loop

M_{ci} Mutual inductance of the feedback control loop and the eddy current

R_c Resistance of the feedback control loop

τ_c Time constant of the feedback control loop

ν_c Conversion coefficient of the loop current to the horizontal field

$G_c(s)$ Gain of the feedback control loop

τ_0 $\tau_0^2 = m_p R_p / I_p B_{v0}$

References

1) A. Fukuyama, et al.: Jpn. J. Appl. Phys. 14 (1975) 871

2) Y. Suzuki, et al.: Proceeding of the 7-th Symposium on Engineering Problems of Fusion Research (1977) 112

3) A. Kameari and Y. Suzuki: Proceeding of the 7-th Symposium on Engineering Problems of Fusion Research (1977) 1386

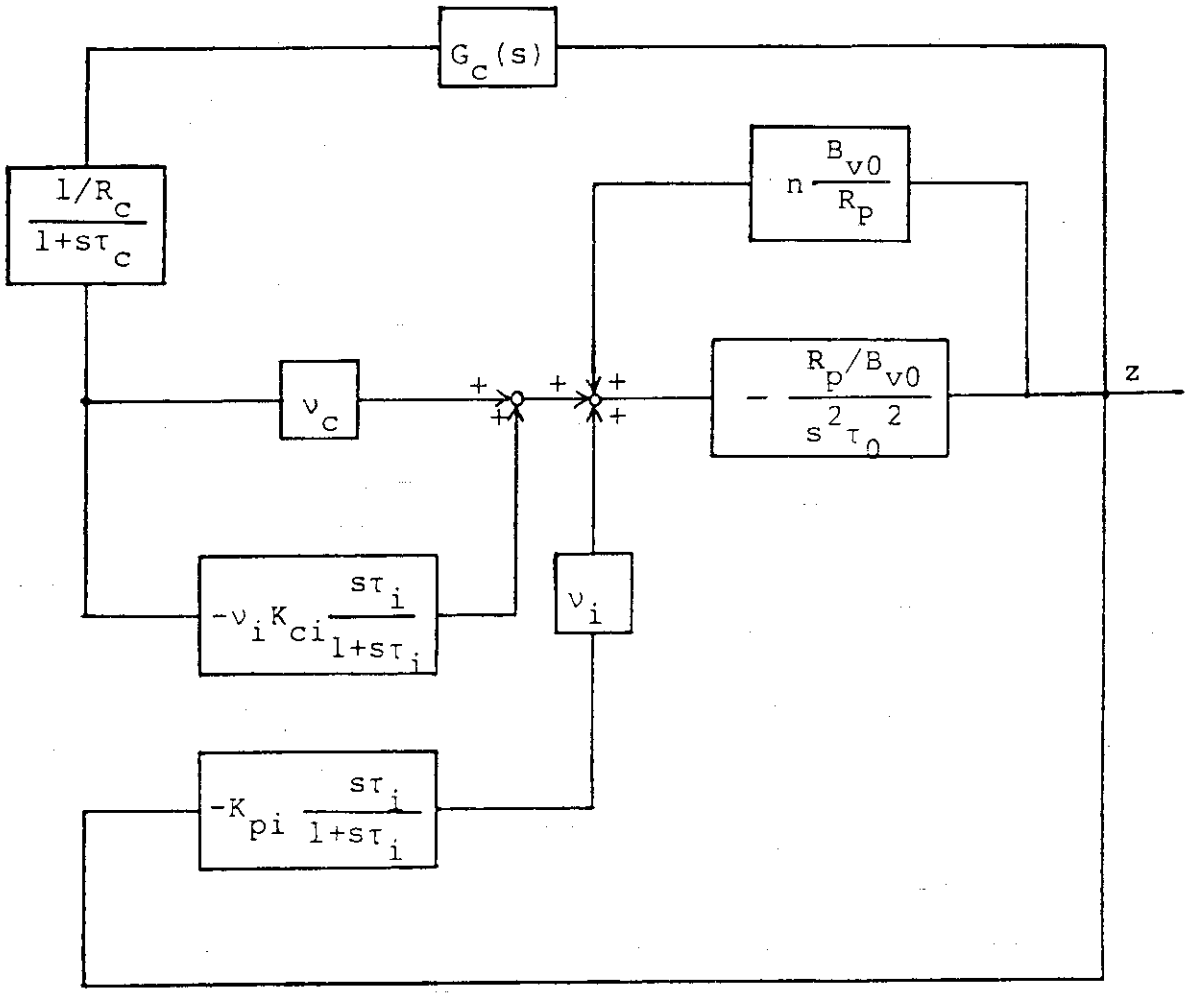

Fig. 5.7 Block diagram of the control system for vertical position.

$$K_{ci}=\frac{M_{ci}}{L_i}\ ,\quad K_{pi}=\frac{\partial M_{pi}}{\partial z}\Big|_{z=0}\frac{I_p}{L_i}$$

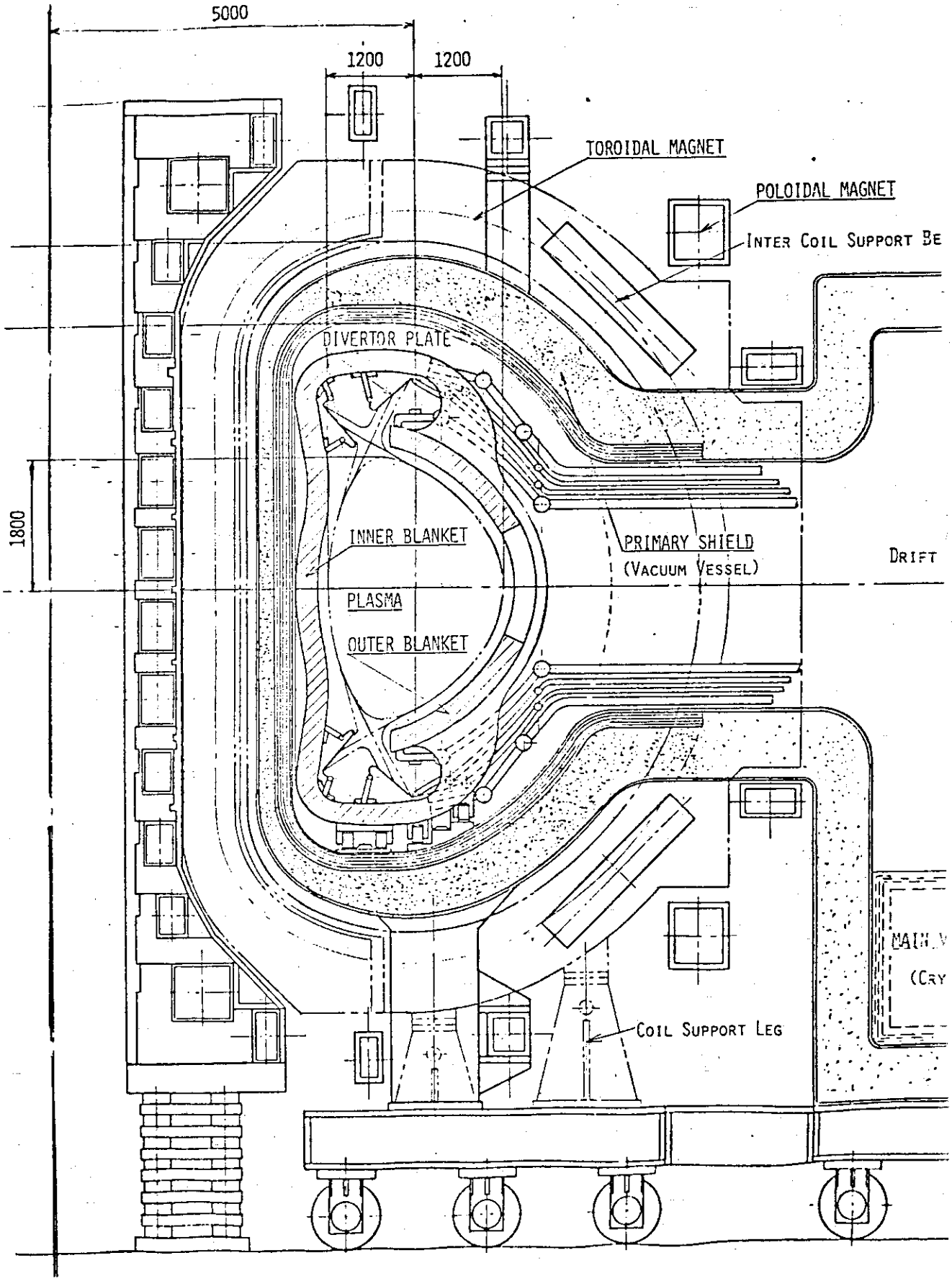

Fig. 5.8 General Reactor Concept of INTOR-J

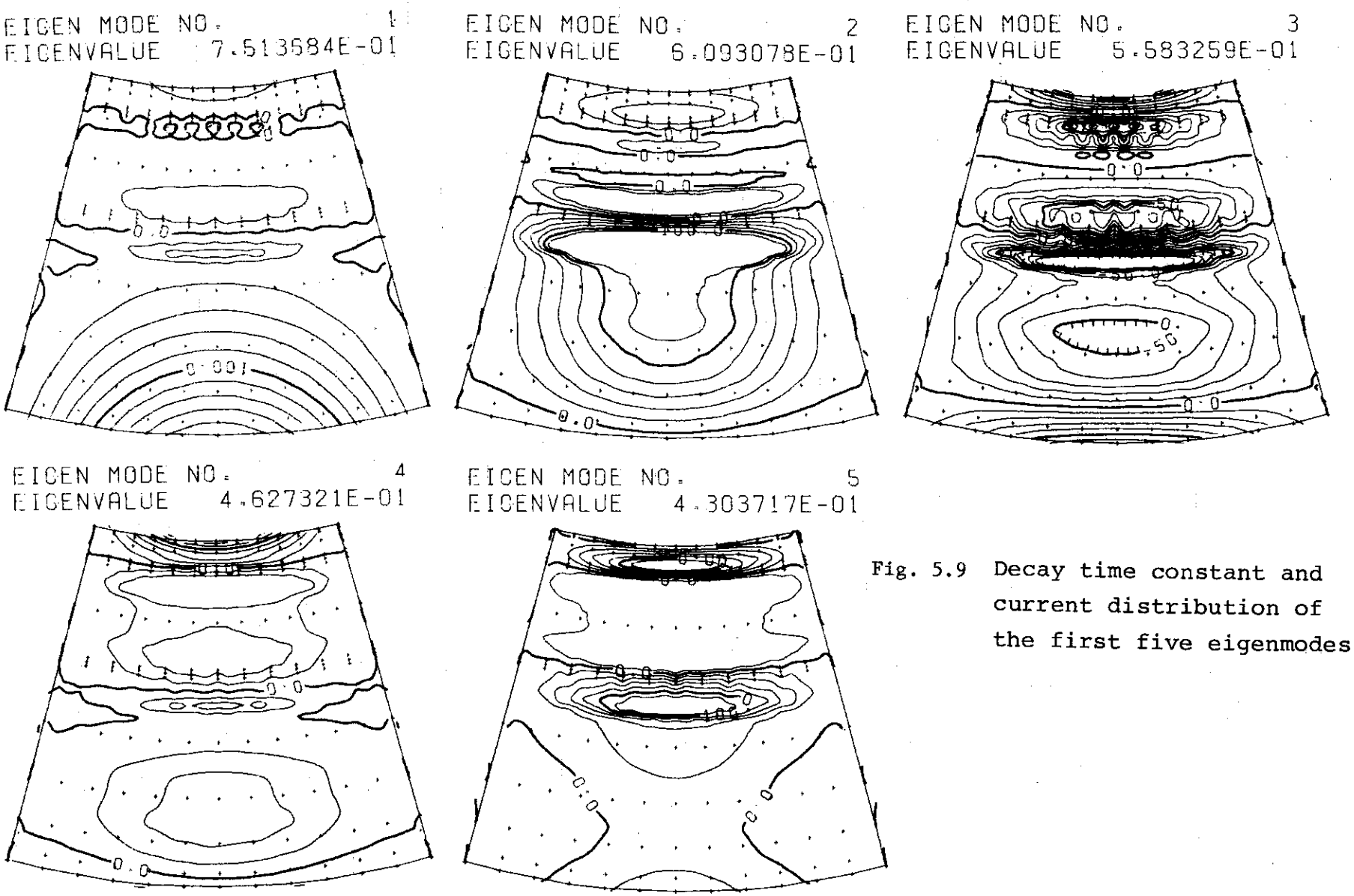

Fig. 5.9 Decay time constant and current distribution of the first five eigenmodes.

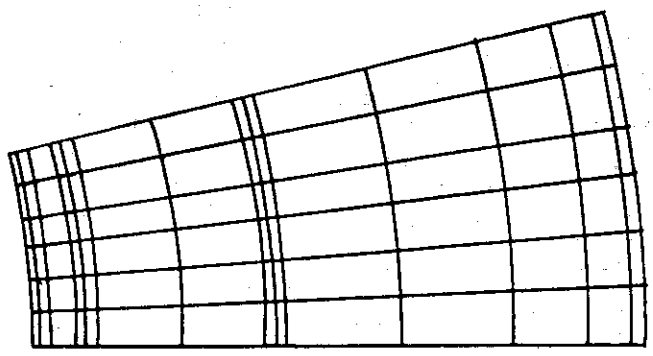

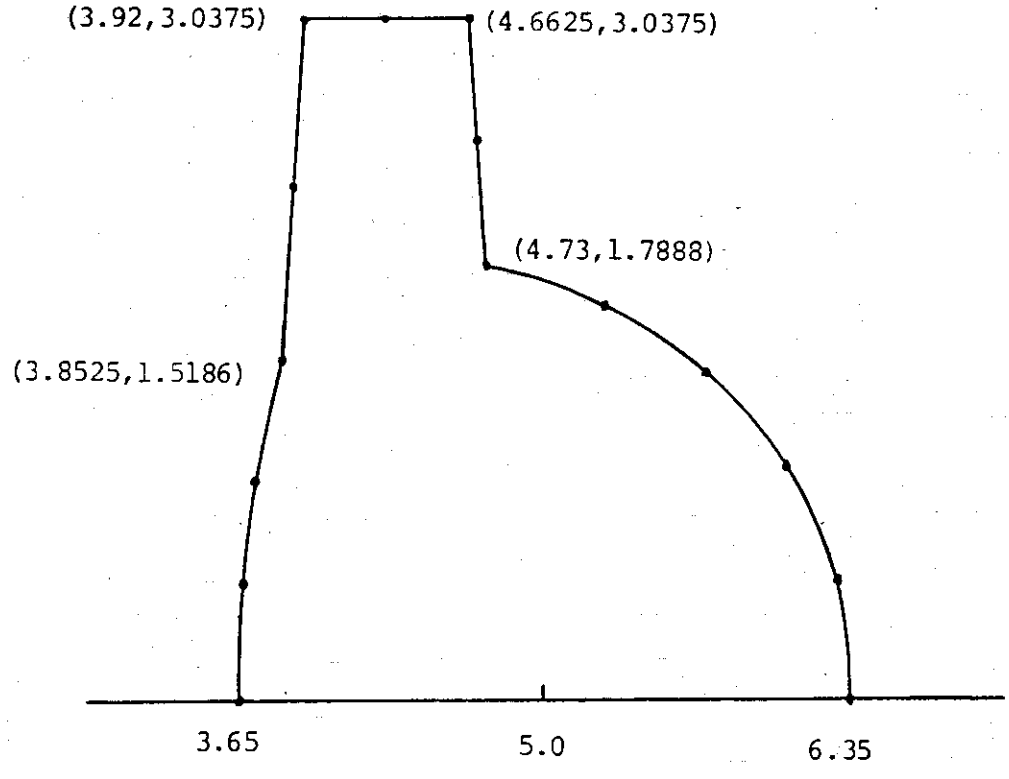

Fig. 5.10 A model of SS blanket with a divertor.

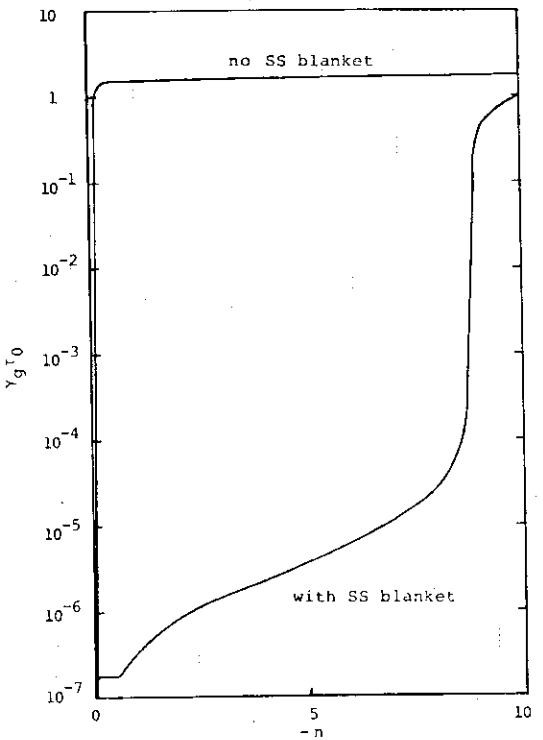

Fig. 5.11 Growth rate of the vertical positional instability.

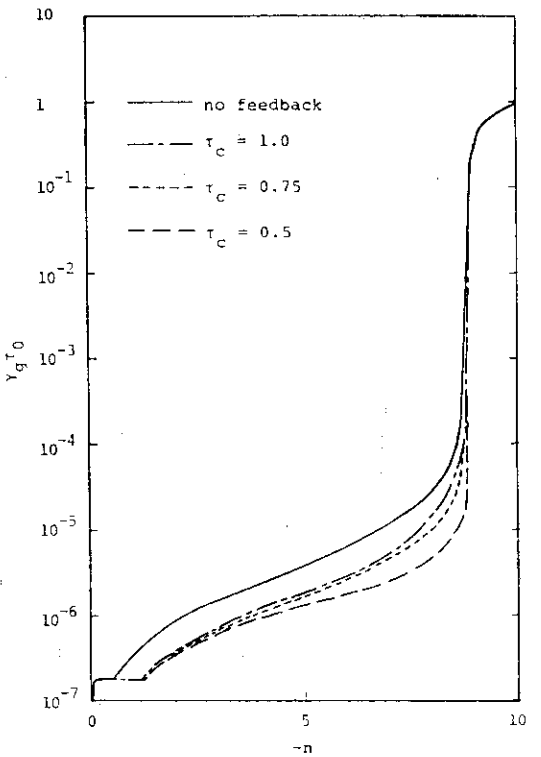

Fig. 5.12 Growth rate of the vertical positional instability with the feedback control, where τ_c is the time constant of the feedback loop. Gain is $0.5G_{0min}$ where G_{0min} is the minimum gain of the feedback loop required for the stabilization of the vertical positional instability.

6. Equilibrium during Current Build-up and Additional Heating

6.1 Current rise with minor radius expansion

During ohmic heating, the plasma current and the density are raised with continuous minor radius expansion by defining the plasma surface with separatrix. The minor radius of the plasma is expanded in such a way that the current density of the plasma, I_p/a^2, remains almost constant ($q_a \simeq 2.5$). In INTOR, the plasma current is raised very slowly ($\simeq$1 MA/s) in order to decrease heat load into super conducting magnets due to eddy current. Because of the long interval during ohmic heating, plasma must be in stable equilibrium or in equilibrium with feedback control. Equilibrium configuration with divertor at each plasma current is shown in Fig. 6.1.

Time evolution of the multipole field components of the equilibrium magnetic field for $\gamma = 0.2$ is shown in Fig. 6.2. Octapole field is necessary for the divertor configuration and seems to play an important role during minor radius expansion. Sharp increase of the hexapole and the octapole field at small plasma current causes high electric power requirement. Therefore free-expansion-like minor radius expansion seems to be favourable in which the plasma shape may not be controlled in the exact manner.

6.2 Additional heating with gradual increase of triangularity

During additional heating to ignition, the poloidal beta increases continuously and almost equal amount of vertical field should be added, so the ampere-turns of the coils must be changed as to keep the plasma in required equilibrium. Fig. 6.3 shows the ampere-turns of I, H and V coils with fixed D coil ampere-turns of 7.6, 4.0 and 2.05 MAT. The location of I, H, V and D coils is shown in Fig. 7.1 of the next section.

Ampere-turns of I and H coils decrease with increasing β_p, if the triangularity of the plasma is hold constant. This is because that less hexapole field is required for higher poloidal beta plasmas and that I and H coils mainly contribute to the formation of the hexapole magnetic field.

From the engineering viewpoint, the ampere-turns of the coils is required to be almost constant because of less electric power and control requirement. Therefore the triangularity of the plasma should be increased gradually as is shown in Fig. 6.3. Only V coil ampere-turns

increases with increasing β_p corresponding associated increase of required vertical field, but need not to be increased so more than the case of the fixed triangularity.

Equilibrium configuration with the without the divertor is shown in Fig. 6.4 and 6.5 for the initial and the final stage of the additional heating.

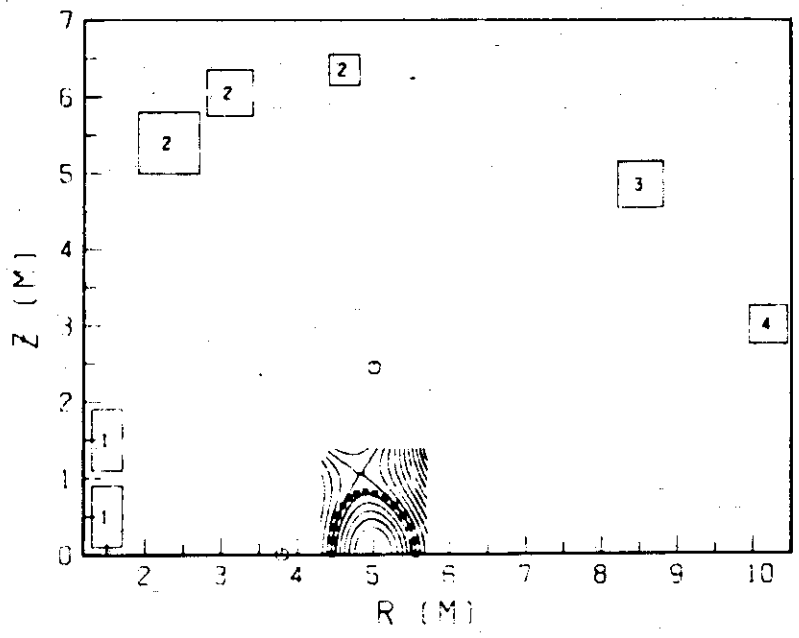

(a) I_p = 1 MA

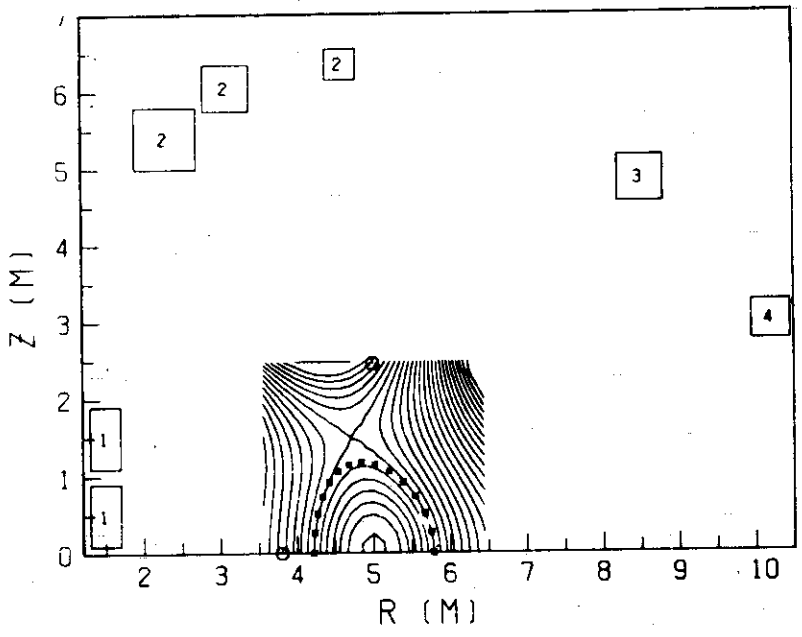

(b) I_p = 2 MA

Fig. 6.1 Equilibrium plasma configuration during minor radius expansion with fixed triangularity γ=0.2 and poloidal beta β_p=0.05.

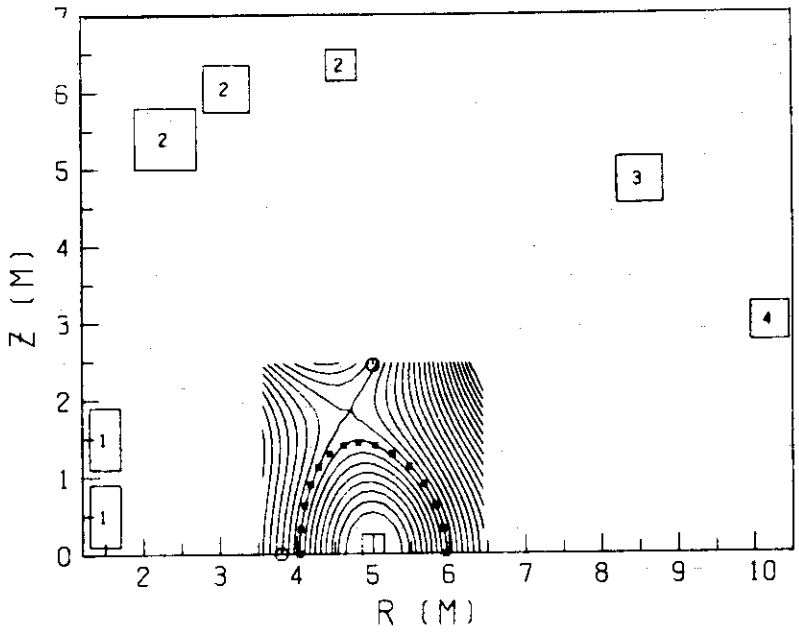

(c) I_p = 3 MA

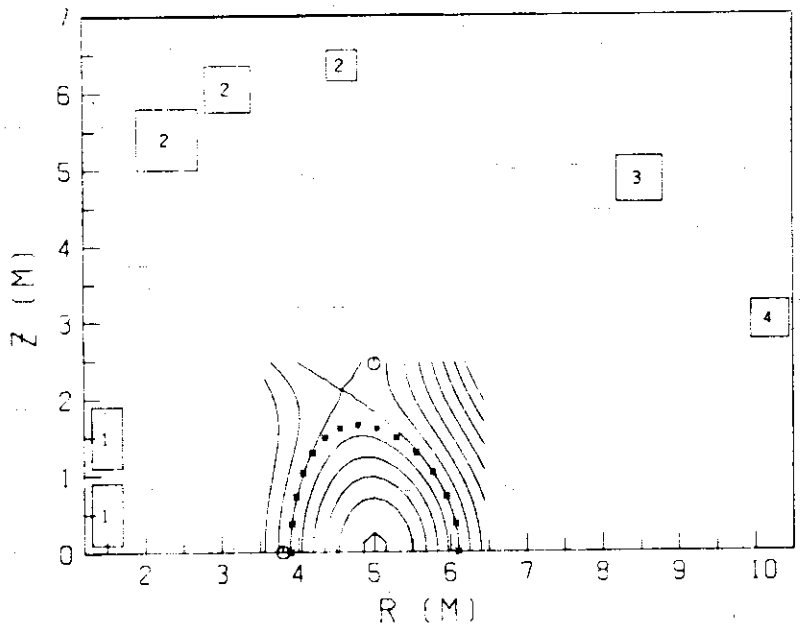

(d) I_p = 4 MA

Fig. 6.1 continued

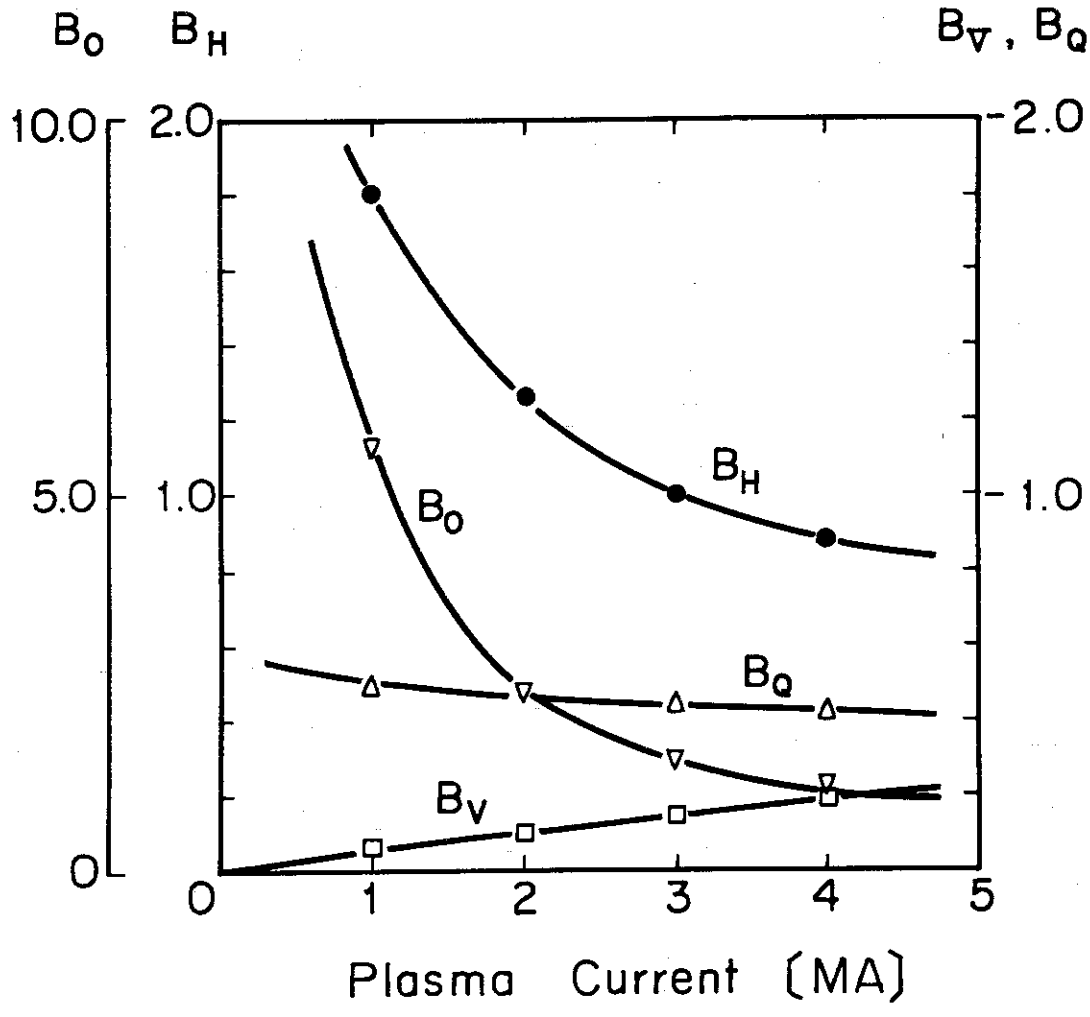

Fig. 6.2 Dependence of multipole magnetic field on the plasma current during minor radius expansion. Octapole field seems to play an important role.

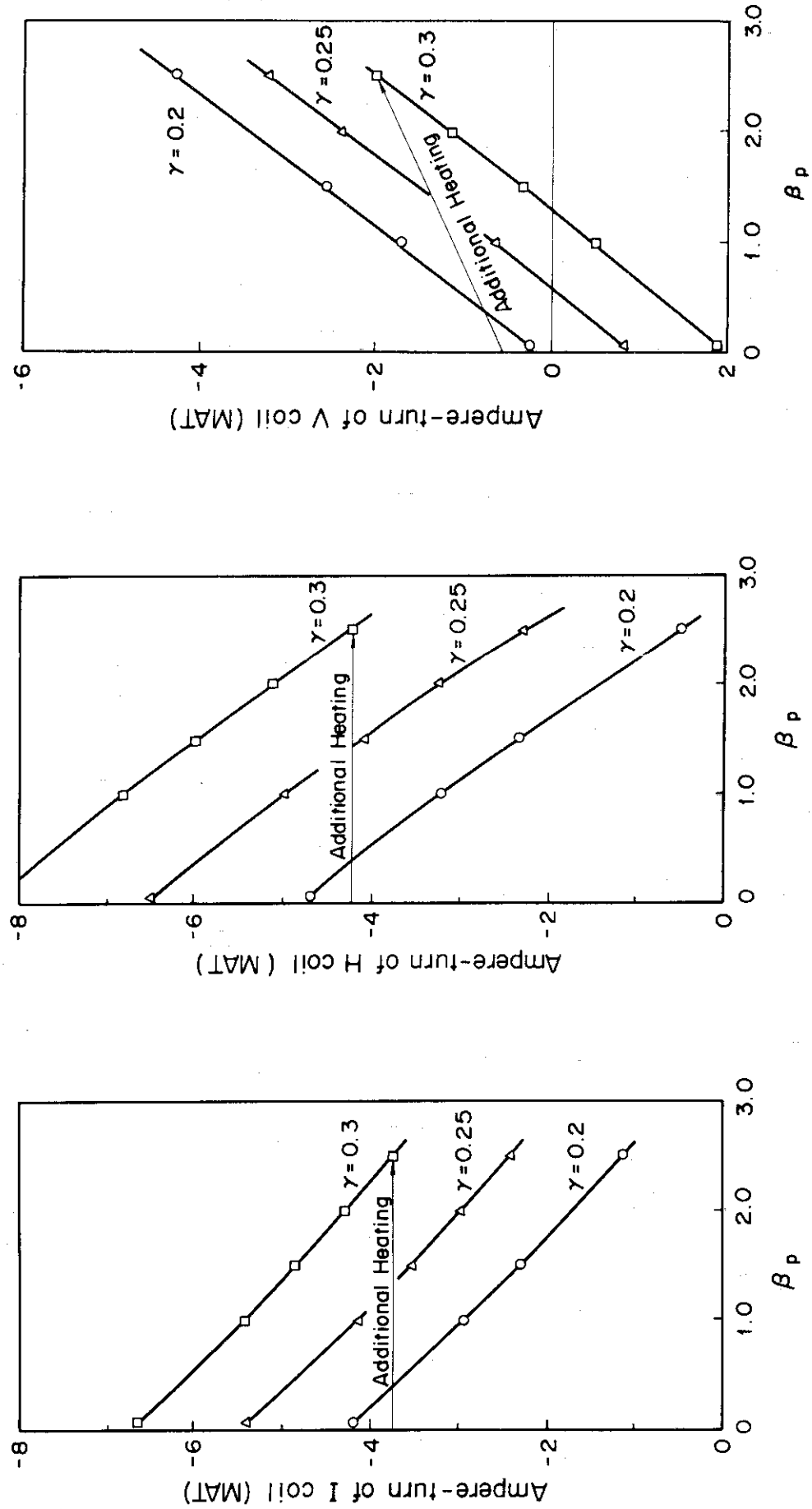

Fig. 6.3 Dependence of the ampere-turns of equilibrium coils on the poloidal beta values. Method of additional heating is also shown corresponding to gradual increase of triangularity in which I coil and H coil ampere-turns are kept constant.

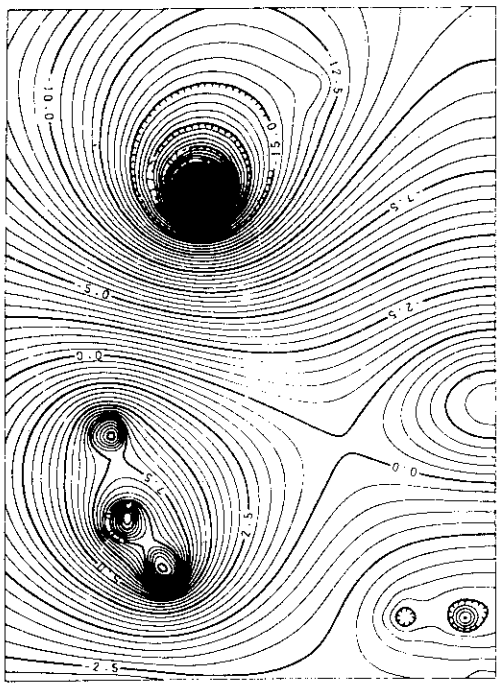

(a) $\beta_p = 0.06$

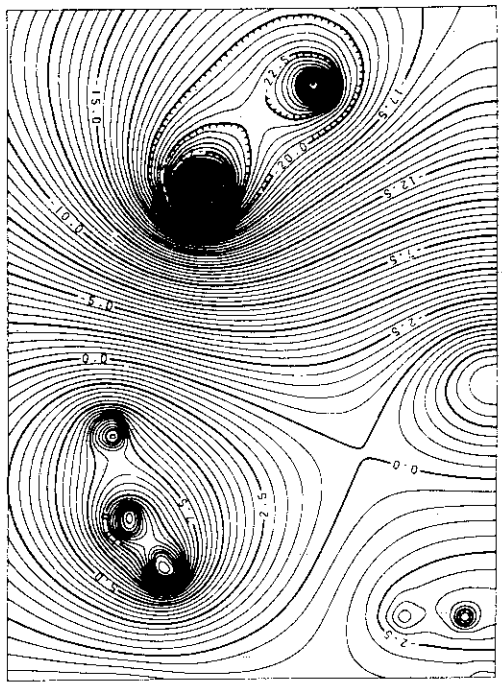

(b) $\beta_p = 2.5$

Fig. 6.5 Equilibrium configuration with divertor.

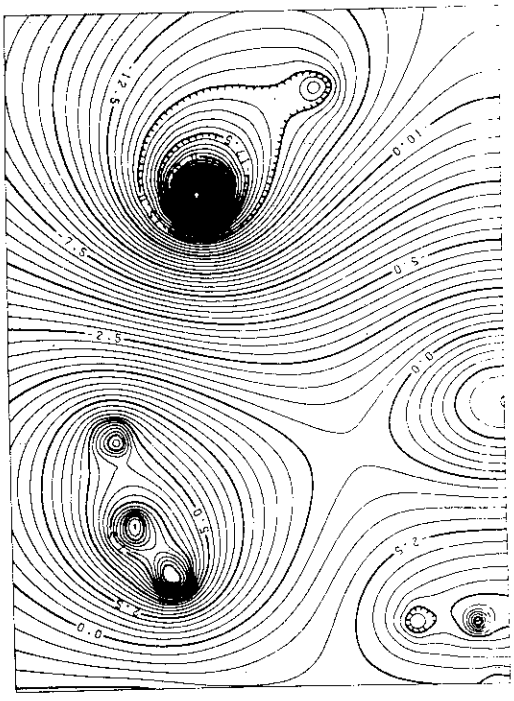

(a) $\beta_p = 0.06$

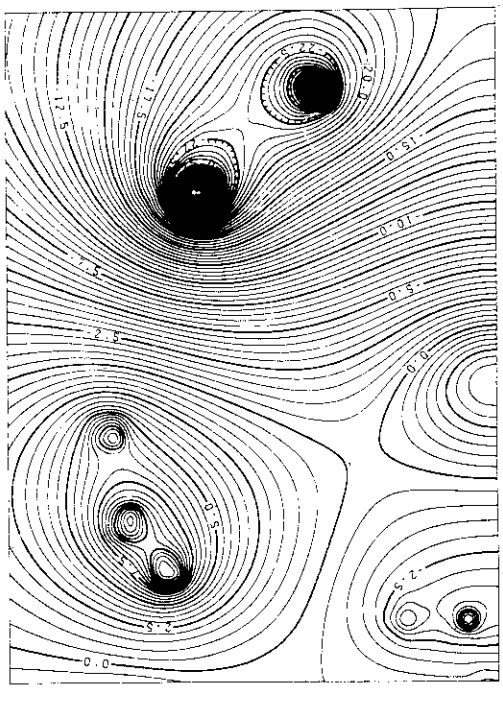

(b) $\beta_p = 2.5$

Fig. 6.4 Equilibrium configuration without divertor.

7. Engineering Aspect and Hardwares

Here we discuss the engineering aspects of the INTOR Poloidal field coil configuration somewhat quantitatively.

7.1 Constraint due to machine structure

7.1.1 Remote maintenance

Remote maintenance mainly limits the design of the INTOR hardwares, especially the design of the poloidal field coils, because of super conducting magnets as toroidal and poloidal field coils and also of large electromagnetic force acting on the coils which requires strong mechanical supports against it. Poloidal field coils placed inside the toroidal field coils (Interior Coil System), especially inboard coils can hardly be replaced or repaired by remote handling. Therefore all poloidal field coils should be placed outside the toroidal field coils (Exterior coil System) for easy remote handling. Plasma shaping is easily achieved by exterior coils, and the stability is also controlled with the aid of long time constant of the inner structure (see Section 5.4).

Exterior poloidal field coil system, all coils of which are placed outside the toroidal field coils, is highly recommended because of its mechanical simplicity and easy remote maintenance, which might be most realistic in the future commercial reactors.

7.1.2 Super conducting magnet

In INTOR, both toroidal and poloidal field coils are planned to be super conducting. This is due to the reduction of the electric power requirement. Eddy current loss in the super conducting magnets due to change of the magnetic field inside them raises heat load into liquid helium, and in turn increases electric power requirement for LHe cooling system. Too much heat load causes that the power required for LHe cryostat system exceeds the saving of joule loss in SC coils. Therefore coils should be designed carefully as to decrease the magnetic field in both toroidal and poloidal field coils, at least rapidly field changing phase. In this reason, current initiation should be done with adequately slow speed, that is, at low voltage and the ohmic heating coils must be placed outside the toroidal field coils, which is the most favourable configuration that would not induce magnetic field inside the toroidal field coils.

7.1.3 Large electromagnetic force

In large tokamaks ampere-turns of the coils tend to increase resulting in the increase of electromagnetic forces up to an intolerable level. To avoid this difficulty, poloidal field coil position should be designed carefully and the ampere-turns should be optimized.

7.1.4 Available electric power

To obtain net electric power from INTOR the electric power and energy input should be lower than a certain level. Hybrid poloidal coil system can reduce the required electric power because it can decrease the total ampere-turns while the power factor of the electric power supply reaches unity (see Report 8).[1)] Energy dissipation can be reduced mainly by the use of super conducting magnets.

Hybrid poloidal coil system also decreases the numbers of poloidal coils resulting in the large access gaps, mechanical simplicity and easy remote maintenance.

Slow plasma current rise is also effective for electric power reduction, especially at the final stage of the current rise with a little additive expense of required volt-seconds.

7.2 Design of hybrid poloidal field coil system

7.2.1 Design process

Hybrid poloidal field coil system has been designed on the following process.

(i) Decide coil locations from the viewpoint of the machine structure and system integration. Sufficient numbers of coils must be equipped to lower the magnetic field leakage in the plasma and in the toroidal field coils during the current initiation stage. At this stage only transformer components of the coil currents flow in the coils.

(ii) Arrange the coils into some parallel connected blocks in which coils are connected in series, the number of the blocks being decided so that it is not less than the number of control objects of the plasma. For example at least four independently controlled coil blocks are necessary for the non-circular plasma with triangular cross section which has four plasma parameters to be controlled, that is, major

and minor radius, ellipticity and triangularity. Plasma current is controlled by adjusting ampere-turns of all blocks simultaneously, hence additive blocks are not necessary, while one more electric power supply is required.

(iii) Decide the number of turns of the coils so that the voltage drops across the blocks become equal when only the transformer currents flow in the coils. (For the detailed understanding of the power supply system, the report of group 8 should be refered.)

(iv) Estimate the ampere-turns of the coil blocks by solving the plasma equilibrium. Total ampere-turns is the sum of the equilibrium and the transformer components. The value of the transformer component should correspond to the flux swing which is the difference between the required volt-seconds and the supplied flux by equilibrium field coil currents.

(v) Optimize the ampere-turns from the engineering viewpoints.

7.2.2 Coil locations

The locations of the poloidal field coils are shown in Fig. 7.1 which have been decided on the bases described in the preceding section. All coils are lumped into 6 parallel-connected blocks in which coils are electrically connected in series. Four coil blocks are used as equilibrium coils which can control the INTOR plasma parameters completely.

7.2.3 Ampere-turns

In this section we decide the ampere-turns of the equilibrium field coils based on the results established in 2.1.

Maximum current density which can be tolerated by the super conducting magnets is estimated at 20 A/mm^2 in the conductor, and decreases to about a half if the current is averaged over the overall cross section including super insulation, supporting structure and others. In INTOR, there left only a little space radially inside the toroidal field coils because of the small major radius of the plasma. Therefore the ampere-turns of the innermost coils (No. 1, 2) should be lower than a certain level. Actually the level is estimated at about 8 MAT. Concerning electromagnetic force acting on these coils, the level should be lowered still more.

A current-carrying plasma can be elongated essentially in two ways- by (a) pulling at the ends or (b) pushing on the sides. In INTOR these two functions are achieved mainly by D coils in the cases of (a) and I coils in the cases of (b). Practically these two functions co-operate, and then the ampere-turns of these coils should be optimized from the engineering viewpoint.

Fig. 7.2 shows the relationships between ampere-turns of I coil and D coil for 2×2 cases of poloidal beta and triangularity. Also shown with the dotted line is the engineering limit described above. At the beginning of the additional heating (β_p=0.06) plasma cannot be shaped to a large triangularity (γ = 0.3). As the ampere-turns of the D coil are raised, separatrix approaches the plasma surface resulting finally in the divertor configuration.

Fig. 7.3 shows the effectiveness of the equilibrium coil current. Effectiveness is defined as the ratio of the supplied flux at the major radius to the stored magnetic energy (VS/E). The figure shows that the effectiveness decreases with increasing D coil ampere-turns. Therefore the ampere-turns of the D coil should not be increased unnecessarily. D coil ampere-turns around 7.5 MAT seeme to be favourable for the non-divertor configuration.

Table 7.1 shows thus decided ampere-turns of the poloidal field coils.

The maximum magnetic field on the conductor surface of the I coil reaches to 8 T when the ampere-turns is increased to about 6.5 MAT, though only a part of the surface radially inside reaches this value. Therefore the Nb_3Sn is inevitable if the more ampere-turns than 6.5 MAT is necessary in order to obtain highly triangular plasma such as γ = 0.5. If the radius of the I coils is increased, the situation can be mitigated because of less ampere-turn requirement for the ohmic heating coils. Then we have more margin for plasma control. Enlargement of the plasma radius by about 50 cm will satisfy the demand.

7.2.4 Magnetic field configuration

Ohmic heating coils should not produce the magnetic field in the toroidal coils and the plasma region. Reduction of the field in these region can easily be done by appropriate arrangement of the coils and the current feed by parallel-connected coil blocks. Field leakage below 800 G at the toroidal field coils can be achieved, and the value dose not

imply the excessive field change during breakdown. Flux lines and surfaces on which the field strength is the same are shown in Fig. 7.4.

Magnetic field configuration produced by the equilibrium field coils is shown in Fig. 7.5.

If the conducting shell cannot be located close to the plasma, feedback controlled external lateral field is necessary to restore the plasma on the mid-plane against unstable vertical derivation. The lateral field can be produced by for example No.2 and No.6 coil blocks. Fig. 7.6 shows the flux lines of the lateral field.

7.2.5 Position of the first wall

The first wall is located by 10 cm away from the plasma surface and the shape is fitted to $\gamma = 0.3$, which is equal to the triangularity of the plasma during burn. Fig. 7.7 shows that the first wall can confine the plasma of wide range of triangularity ($\gamma = 0.2$-0.4) without intercepting the plasma surface.

Reference

1) JAERI-M 8511 (1979) IAEA INTOR WORKSHOP REPORT, GROUP 8
—— Power Supply and Transfer ——

Table 7.1 INTOR Poloidal Field Coil Locations and Maximum Ratings

Coil No.	Blok No.	Function	R (M)	Z (M)	N (Turns)	OHC Component (MAT)	Shaping Component (MAT)	Total (MAT)	OHC Component (MAT)	Shaping# Component (MAT)	Total (MAT)
							without divertor			with divertor	
1	1	I_1	1.5	0.5	75	-2.60	-3.77	-6.37	-3.23	-2.98	-6.21
2	1	I_2	1.5	1.5	74	-2.57	-3.72	-6.29	-3.19	-2.94	-6.13
3	2		1.5	2.5	54	-2.67	*****	-2.67	-3.33	*****	-3.33
4	2		1.575	3.5	49	-2.45	*****	-2.45	-3.04	*****	-3.04
5	2		1.665	4.5	47	-2.35	*****	-2.35	-2.92	*****	-2.92
6	3	D_1	2.3	5.4	74	-1.29	7.6	6.31	-1.61	9.1	7.49
7	3	D_2	3.1	6.05	39	-0.68	4.0	3.32	-0.84	4.78	3.94
8	3	D_3	4.6	6.35	20	-0.34	2.05	1.71	-0.43	2.47	2.04
9	4		6.25	6.1	127	-0.17	*****	-0.17	-0.21	*****	-0.21
10	5	H	8.5	4.85	127	-0.10	-4.23	-4.33	-0.12	-4.79	-4.45
11	6	V	10.2	3.0	125	-0.08	-1.98	-2.06	-0.10	-1.68	-2.16

Plasma current I_p at the flat-top is 4.7 MA.

Triangularity γ = 0.3 is assumed.

#...Divertor case is not the result of systematic study.

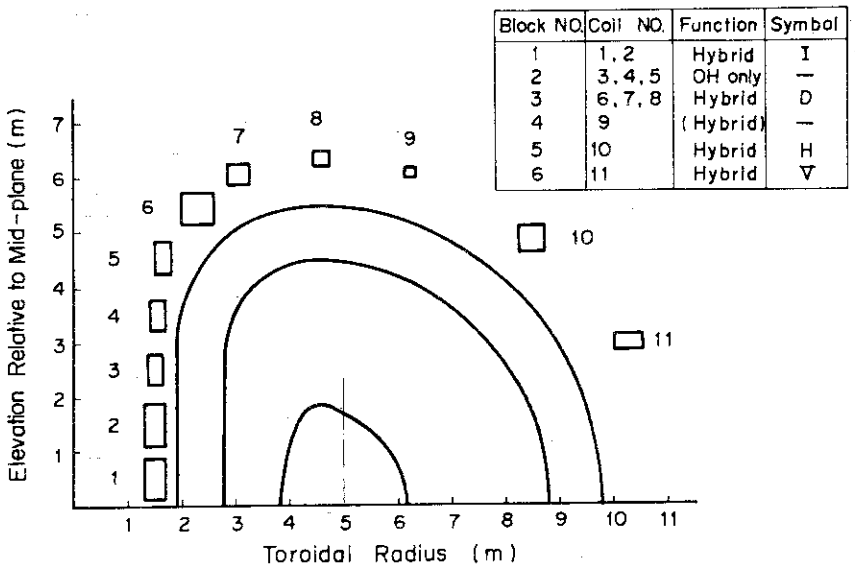

Fig. 7.1 INTOR Hybrid Poloidal Coil Locations

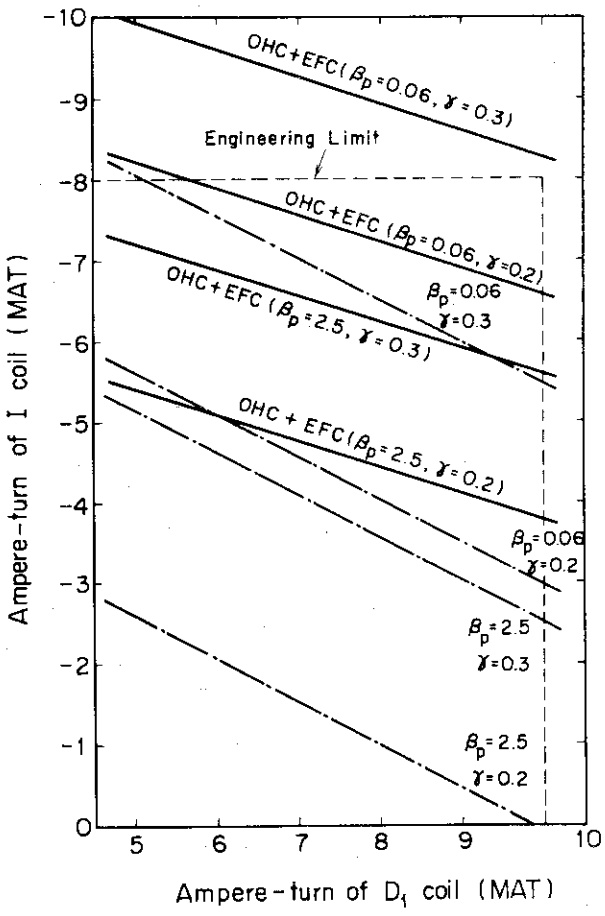

Fig. 7.2 Relation between I coil ampere-turns and D_1 coil ampere-turns for 2×2 cases of poloidal beta (0.06, 2.5) and triangularity (0.2, 0.3). (— - — EFC only)

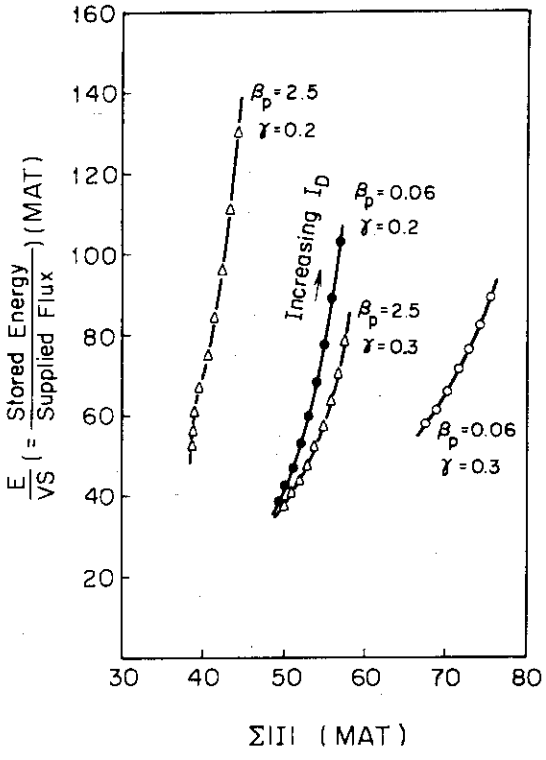

Fig. 7.3 Dependence of inverse effectiveness on the total ampere-turns.

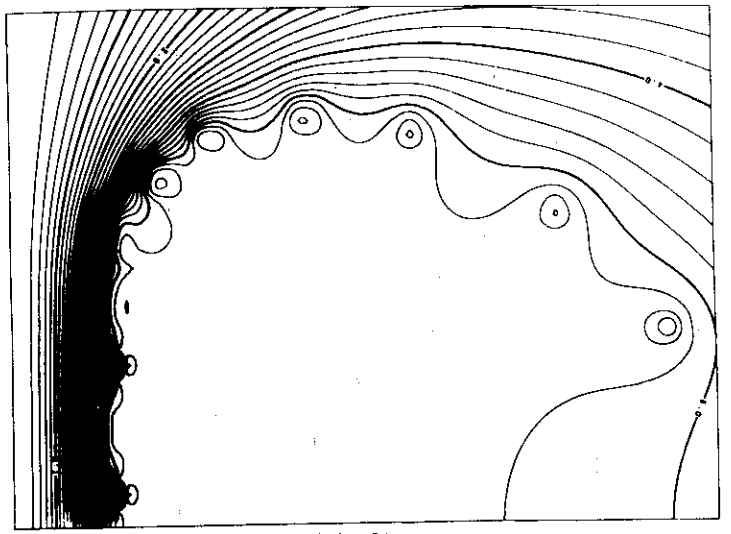

(a) flux

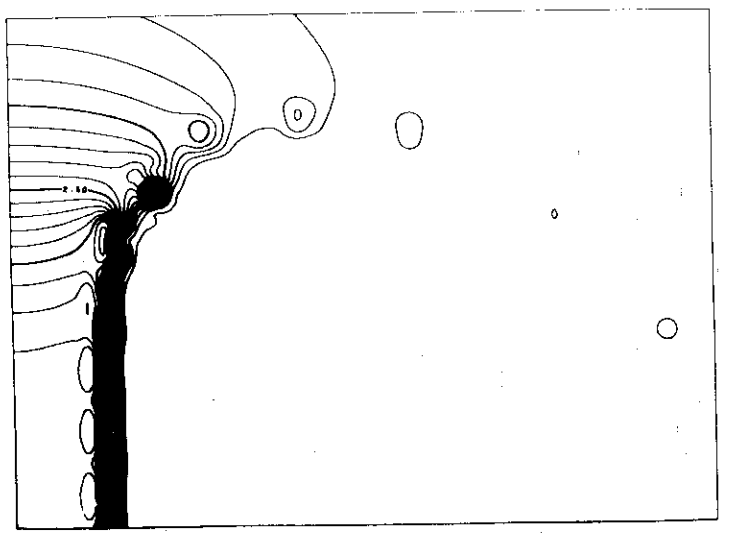

(b) field

Fig. 7.4 Magnetic field configuration and the surfaces of equal field strength of ohmic heating coils.

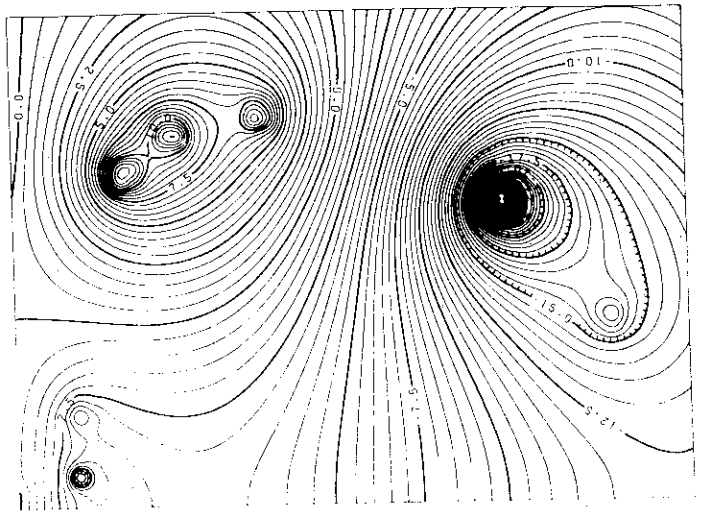

(a) $\beta_p = 0.06$

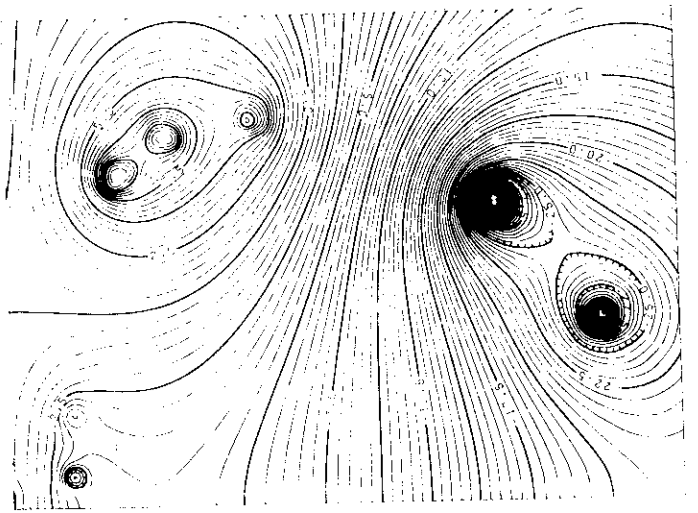

(b) $\beta_p = 2.5$

Fig. 7.5 Magnetic field configuration of equiliblium field coils without divertor.

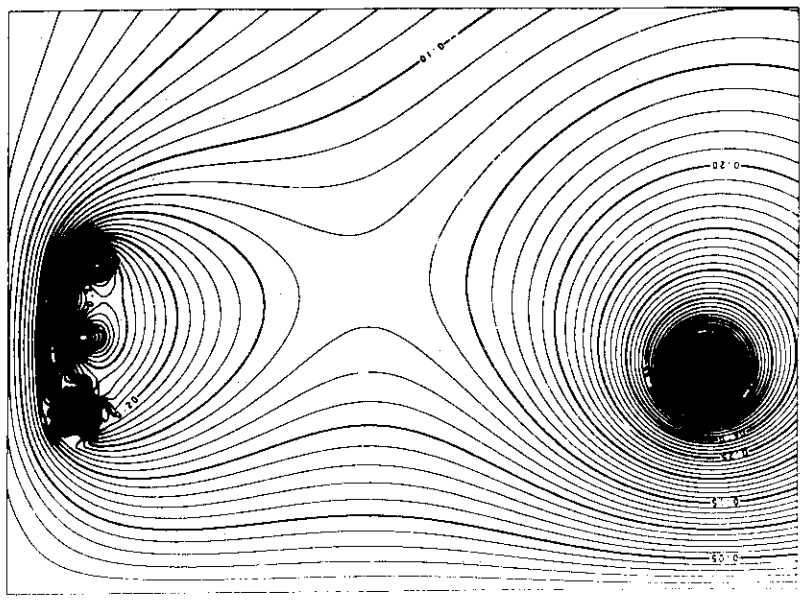

Fig. 7.6 Lateral magnetic field configuration for slow plasma control against vertical displacement. No.2 and 6 coil blocks are used.

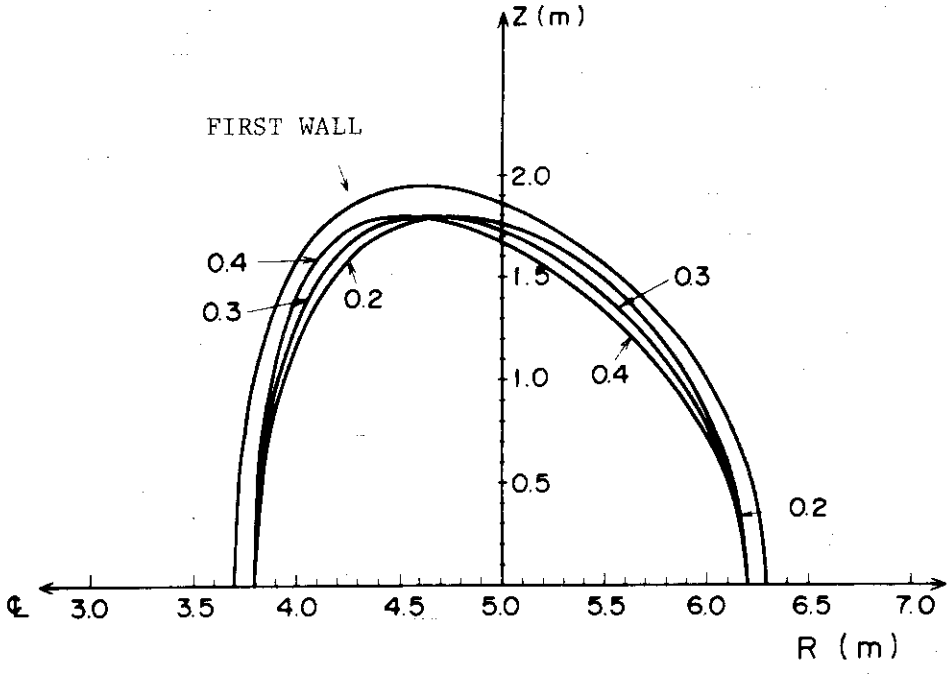

Fig. 7.7 Shape of first wall showing that it can confine plasmas of wide range of triangularity ($\gamma = 0.2 \sim 0.4$).

7.3 $\dot{B}$ and electric power requirement

The maximum magnetic field and the rate of field change on the toroidal and the poloidal field coils are listed in the Table 7.2 at each time step corresponding to the operational scenario shown in Fig. 7.8. Required MG power output is also shown in the table, though the power requirement does not correspond to ampere-turns listed in Table 7.1 exactly.

Rate of field change is not remarkably large and the super conducting magnets would stand the values.

Electric power requirement is rather small due to savings in the joule loss in the super conducting coils and also due to the slow increase of the plasma current especially at the final stage of the current rise.

Table 7.2 Time History of B and MG Power Output

I_p		Breakdown → 0.6MA	0.6 → 4.7MA	Additional Heating	Burn (Divertor Swing)	Shutdown
Time Scale		sec -0.1 → 0.1	0.1 → 5 sec	5 → ∿10 sec	10 → 200 sec	200 → (205∿210) sec
TFC	B max or ΔB	<0.08 T	1.5 T (ΔB = 1.5 T)	1.6 T	1.6 T (ΔB = 0.05 T)	ΔB = 1.6 T
	B max	<0.8 T/S	0.3 T.S		(0.1 T/S)	0.32 T/S
PFC	B max or ΔB	5.5 T	ΔB = 9.4 T	7.5 T	7.5 T (ΔB = 1.3 T)	ΔB = 7.5 T
	B max	6.5 T/S	1.9 T/S		(2.6 T/S)	1.6 T/S
MG Power Output	Divertor Swing	200 MW	650 MW	40 MW	300 MW	-500 MW
	Non-Divertor	300 MW	450 MW	40 MW	40 MW	-350 MW

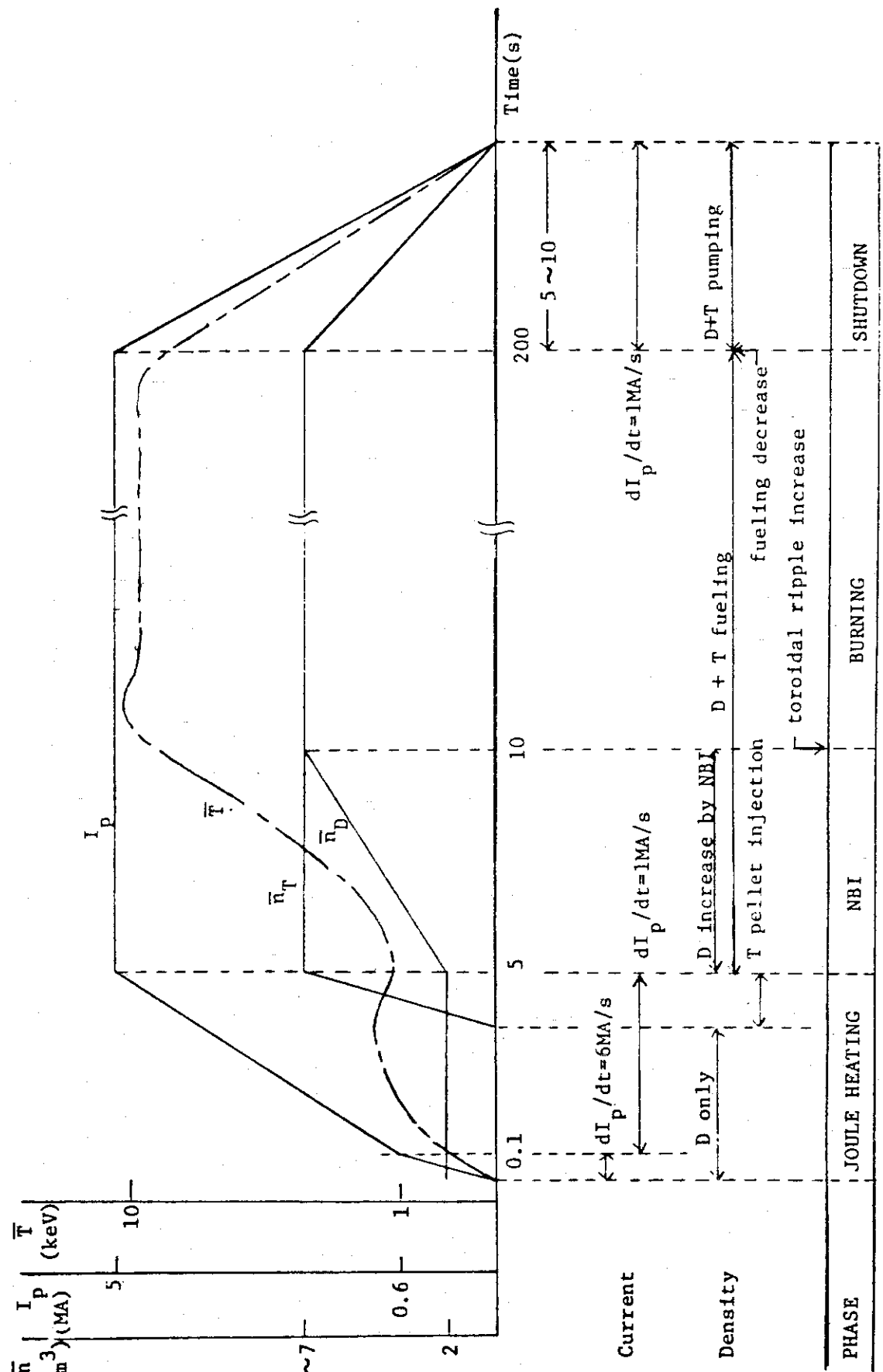

Fig. 7.8 Operational Scenario